

**NAVAL POSTGRADUATE SCHOOL
Monterey, California**



THESIS

**DYNAMIC SYSTEM IDENTIFICATION AND MODELING
OF A ROTARY WING UAV FOR STABILITY AND
CONTROL ANALYSIS**

by

Matthew D. McEwen

June 1998

Thesis Advisor:
Second Reader:

Russ Duren
E. Roberts Wood

Approved for public release; distribution is unlimited.

19980727 177

REPORT DOCUMENTATION PAGE

Form Approved
OMB No. 0704-0188

Public reporting burden for this collection of information is estimated to average 1 hour per response, including the time for reviewing instruction, searching existing data sources, gathering and maintaining the data needed, and completing and reviewing the collection of information. Send comments regarding this burden estimate or any other aspect of this collection of information, including suggestions for reducing this burden, to Washington headquarters Services, Directorate for Information Operations and Reports, 1215 Jefferson Davis Highway, Suite 1204, Arlington, VA 22202-4302, and to the Office of Management and Budget, Paperwork Reduction Project (0704-0188) Washington DC 20503.

1. AGENCY USE ONLY (Leave blank)		2. REPORT DATE June 1998	3. REPORT TYPE AND DATES COVERED Master's Thesis	
4. TITLE AND SUBTITLE DYNAMIC SYSTEM IDENTIFICATION AND MODELING OF A ROTARY WING UAV FOR STABILITY AND CONTROL ANALYSIS			5. FUNDING NUMBERS	
6. AUTHOR(S) McEwen, Matthew D.			8. PERFORMING ORGANIZATION REPORT NUMBER	
7. PERFORMING ORGANIZATION NAME(S) AND ADDRESS(ES) Naval Postgraduate School Monterey, CA 93943-5000			10. SPONSORING / MONITORING AGENCY REPORT NUMBER	
9. SPONSORING / MONITORING AGENCY NAME(S) AND ADDRESS(ES)			10. SPONSORING / MONITORING AGENCY REPORT NUMBER	
11. SUPPLEMENTARY NOTES The views expressed in this thesis are those of the author and do not reflect the official policy or position of the Department of Defense or the U.S. Government.				
12a. DISTRIBUTION / AVAILABILITY STATEMENT Approved for public release; distribution is unlimited.			12b. DISTRIBUTION CODE	
ABSTRACT (maximum 200 words) This thesis presents a method for the dynamic system identification and simulation model development of a small rotary wing UAV. Using aerodynamic parameterization and linear state-space modeling techniques, the Bergen Industrial UAV was modeled for computer simulation to analyze its inherent stability and control characteristics. The NPS designed JANRAD software was utilized to determine the stability and control derivatives used in the simulation model. The identification of the UAV dynamic model will aid in the development of closed-loop controllers capable of autonomous UAV control. The fidelity of the simulation model was verified by comparing the simulation responses with data collected from on-board sensors during test flight				
14. SUBJECT TERMS Unmanned Aerial Vehicles, Stability and Control, Modeling, Simulation, System Identification, Rotary Wing, Helicopter, JANRAD			15. NUMBER OF PAGES 89	
17. SECURITY CLASSIFICATION OF REPORT Unclassified			16. PRICE CODE	
18. SECURITY CLASSIFICATION OF THIS PAGE Unclassified		19. SECURITY CLASSIFICATION OF ABSTRACT Unclassified		20. LIMITATION OF ABSTRACT UL

NSN 7540-01-280-5500

Standard Form 298 (Rev. 2-89)
Prescribed by ANSI Std. Z39-18

Approved for public release; distribution is unlimited

**DYNAMIC SYSTEM IDENTIFICATION AND MODELING OF A ROTARY
WING UAV FOR STABILITY AND CONTROL ANALYSIS**

Matthew D. McEwen
Major, United States Marine Corps
B.S., San Diego State University, 1985

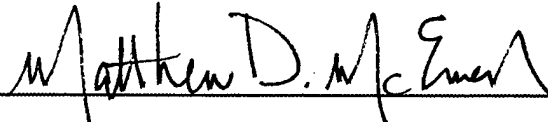
Submitted in partial fulfillment of the
requirements for the degree of

MASTER OF SCIENCE IN AERONAUTICAL ENGINEERING

from the

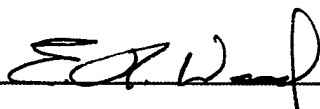
**NAVAL POSTGRADUATE SCHOOL
June 1998**

Author:

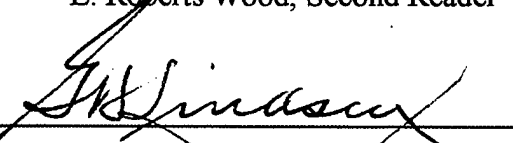

Matthew D. McEwen

Approved by:


Russ Duren, Thesis Advisor



E. Roberts Wood, Second Reader


Gerald H. Lindsey, Chairman
Department of Aeronautics and
Astronautics

ABSTRACT

This thesis presents a method for the dynamic system identification and simulation model development of a small rotary wing UAV. Using aerodynamic parameterization and linear state-space modeling techniques, the Bergen Industrial UAV was modeled for computer simulation to analyze its inherent stability and control characteristics. The NPS designed JANRAD software was utilized to determine the stability and control derivatives used in the simulation model. The identification of the UAV dynamic model will aid in the development of closed-loop controllers capable of autonomous UAV control. The fidelity of the simulation model was verified by comparing the simulation responses with data collected from on-board sensors during test flights.

TABLE OF CONTENTS

I.	INTRODUCTION	1
	A. BACKGROUND	1
	B. APPROACH TO THE PROBLEM	1
II.	MODELING AND SIMULATION	5
	A. ANALYSIS THEORY	5
	B. UAV DESCRIPTION	5
	C. EQUATIONS OF MOTION	7
	D. LINEARIZATION	9
	E. STABILITY DERIVITIVES	10
	F. SOFTWARE (JANRAD)	10
	G. SIMULATION MODEL	11
III.	INPUT PARAMETERS	15
	A. PHYSICAL MEASUREMENTS	15
	B. MOMENTS OF INERTIA	15
	C. ROTOR FLAPPING MOMENT	17
	D. EFFECTIVE HINGE OFFSET	18
	E. AERODYNAMIC INPUTS	21
	F. CONTROL RIGGING DIAGRAMS	23
IV.	SIMULATION ANALYSIS	27
	A. JANRAD IN HOVER	27
	1. Performance Calculations	27
	2. Stability Analysis	28
	B. SIMULINK MODEL IN HOVER	35
V.	FLIGHT TESTING	43
	A. INSTRUMENTATION OF FLIGHT VEHICLE	43
	B. PHYSICAL PARAMETER MODIFICATION	43
	1. Center of Gravity	44
	2. Moments of Inertia	44
	3. JANRAD Input Modifications	45

C.	REQUIRED MODIFICATIONS TO OUTPUT DATA	46
1.	Data Translations	46
2.	Vibration Noise Elimination	47
D.	FLIGHT DATA ANALYSIS	47
E.	COMPARISON OF SIMULATION AND FLIGHT DATA	50
VI.	CONCLUSIONS AND RECOMMENDATIONS	59
A.	CONCLUSIONS	59
B.	RECOMMENDATIONS	60
	APPENDIX A. STABILITY AND CONTROL DERIVATIVES	61
	APPENDIX B. JANRAD INPUT DATA	63
	APPENDIX C. MASS-MOMENTS OF INERTIA CALCULATIONS	67
	APPENDIX D. BEAM DEFLECTION EXPERIMENTAL DATA	69
	APPENDIX E. STATE-SPACE MATRICES	71
	APPENDIX F. CENTER OF GRAVITY AND MOMENT OF INERTIA	73
	LIST OF REFERENCES	75
	INITIAL DISTRIBUTION LIST	77

ACKNOWLEDGMENT

The author would like to express his sincere gratitude to the faculty and staff at the Naval Postgraduate School for the assistance provided in the research and preparation of this thesis. Special thanks to Professor Russ Duren for the time, patience and advice provided during this endeavor. Appreciation also goes out to Professor Wood for his help and council with rotary wing matters; and to Mr. Don Meeks for his professional flying skills and technical assistance over the past nine months.

Most importantly, I would like to thank my wife and children for their understanding, patience and support during this demanding period.

I. INTRODUCTION

A. BACKGROUND

"Everybody's simulation model is guilty until proved innocent."

(Thomas H. Lawrence at the 50th Annual
Forum of the AHS, Washington, 1994)

Computer simulation use by the aerospace engineer is beneficial in preliminary design, stability and control analysis, and handling qualities determination for air vehicles. Automatic control systems enable the stability and handling qualities of an aircraft to be augmented to increase performance. With the addition of onboard sensors tied to a feedback control system, autonomous flight is possible, and is widely used today on a variety of Unmanned Air Vehicles (UAV) within the DoD. Control design theory requires a thorough knowledge of the system to be controlled. When dealing with the control of air vehicles, an improper design can lead to catastrophic results; therefore, accuracy in the characterization of the system to be controlled will facilitate the design process enabling us to "model" the aircraft prior to breaking the earthly bounds. The Naval Postgraduate School has conducted extensive research in the design of a variety of feedback controllers for the Bluebird and FROG fixed-wing UAVs, in addition to the Archytas, VTOL air vehicle. To further research in this area, NPS has obtained a Bergen Industrial rotary-wing UAV to conduct similar studies in this field by the use of feedback controllers.

B. APPROACH TO THE PROBLEM

In the past, control of UAVs was conducted primarily by a ground-based pilot using a standard radio controller (RC) where each task had to be monitored by the ground pilot for the duration of the flight. With the advent of the global positioning system (GPS), the UAV's position can be tracked electronically vice relying on video imaging projected from the UAV to the ground station. Incorporating onboard sensors, feedback controllers

or autopilots can now be used to maintain UAV control without full time pilot inputs. The Predator UAV can operate autonomously for up to 24 hours using pre-planned routes or near-real-time course changes all using onboard sensors to track aircraft position. The Naval Postgraduate School has developed UAV controllers which can be controlled autonomously or via voice command using a “wearable” voice recognition PC unit. The Bergen Industrial Twin UAV (Figure 1.1) was acquired to continue air vehicle control research with the ultimate goal of using video imaging to control the autonomous flight of a rotary wing air vehicle. Prior to developing a controller for the UAV for autonomous

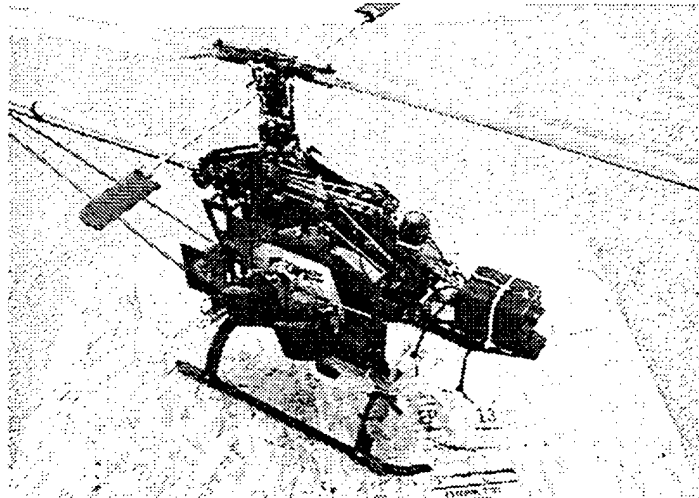


Figure 1.1 Bergen Industrial Twin UAV

flight, it was desired to obtain a mathematical model capable of simulating the air vehicle’s response to controller inputs. This paper outlines the effort of the author to obtain an accurate model of the UAV by using aerodynamic parameterization. Additionally, it provides a method by which a similar modeling and verification process can be conducted on similar scale rotary-wing UAVs. It is assumed the reader has an understanding of helicopter aerodynamics, aircraft stability and control, and basic system control theory. The references recognized throughout this paper provide an excellent source for conducting further research.

To accomplish the simulation modeling, the following approach was utilized:

- 1) Determine UAV physical parameters
- 2) Determine stability derivatives
- 3) Develop simulation model
- 4) Perform flight testing to verify computer model fidelity.

Using physical measurements, experimental testing and similarity analysis, or table look-up, the UAV can be “parameterized” in order to conduct a performance and stability analysis. From this physical parameterization of the air vehicle, we wish to develop a simulation model capable of conducting frequency and time-response analysis. To perform this analysis, it was necessary to characterize the air vehicle system or “plant”. To obtain the stability and control derivatives, the NPS developed Joint Army/Navy Rotorcraft Analysis and Design (JANRAD) software program was utilized in the determination of modeling parameters and frequency response analysis. Finally, the fidelity or accuracy of the simulation model can be verified by conducting flight testing with an instrumented UAV to obtain aircraft response data for comparison with the simulation data. The flight-testing conducted was restricted to a hover due to mechanical and structural problems experienced during the research process. It is the goal of the author that, through the verification/modification of the simulation model, this work can be used for future autonomous controller design.

II. MODELING AND SIMULATION

A. ANALYSIS THEORY

A mathematical simulation model of a helicopter's flight dynamics must include the important aerodynamic, structural and other integral dynamic effects that combine to influence the aircraft's response to pilot inputs. The flight dynamics of the helicopter is described by a complex, non-linear, nine degree-of-freedom (DOF) system. Describing the helicopter's flight dynamics is a difficult task, but developing an accurate mathematical model presents an even greater challenge. A widely used approximation for describing the helicopter's behavior is the linearized, six DOF system. The linearized model is adequate for analyzing small perturbations ($\pm 15^\circ$) about a trim condition. For an in-depth development of the linearized model, the reader is referred to Reference 1. A general overview is presented below.

B. UAV DESCRIPTION

Future utilization of the selected air vehicle requires the capability to accommodate a sizeable payload. Additionally, the initial purchase cost must not be prohibitive within the constraints of the research budget. Past UAV projects have benefited from the generosity of excess military platforms, such as the Bluebird and the Frog. The Bergen industrial UAV was designed as an Industrial platform capable of handling camera equipment for aerial photography. Its advertised payload of 20 pounds was within the desired scope for handling the onboard telemetry required for the control research envisioned by the thesis advisor.

The UAV designer uses off-the-shelf components for the fuselage and rotor systems. In order to increase the UAV's payload capacity, the standard single-cylinder Zenoah engine was modified into a dual-cylinder engine (hence the name Industrial Twin). The increased compression (torque) inherent in a dual-cylinder engine was more than the

standard (single-cylinder) pull-starter could handle leading to several flight schedule setbacks due in part to a broken starter. The RC helicopter is controlled in the same manner as a standard single-rotor helicopter; thrust is controlled by main rotor collective pitch, longitudinal pitch and roll are controlled by main rotor cyclic (longitudinal and lateral, respectively), and directional control (and anti-torque) are controlled by the tail rotor. The UAV is controlled by an outside pilot via remote control using a standard RC transmitter, receiver and electric-control servos. Each of the four control inputs receives a separate signal to control the appropriate on-board control servo which in turn actuates the appropriate control surface (changes blade pitch either cyclically or collectively). The transmitted signal from the Futaba[®] controller is in the form of a pulse width modulation, or PWM signal.

The similarities of the UAV and conventional, full-size helicopter end when we discuss the operation of the main rotor system. Like the full scale helicopter, main rotor collective is controlled by changing the rotor pitch on all blades simultaneously, or collectively, by the uniform movement of the swashplate, but rotor cyclic control is slightly different. The Bergen industrial incorporates the Hiller rotor head system (Figure 2.1). The rotational inertia of the UAV main rotor is too much for the small servo

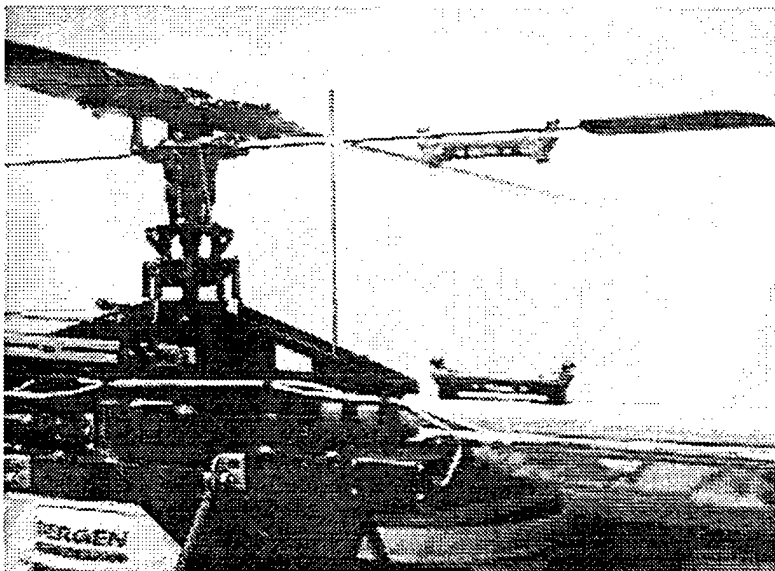


Figure 2.1 Hiller Rotor System

actuators to overcome when an aircraft attitude change is demanded. Therefore, the cyclic control servos deflect the Hiller paddles, which either increase or decrease their angle of attack (AOA). As the AOA is changed, the lift on the paddles will increase causing the flybar to flap up or down (depending on the input). As the flybar flaps, it will change the orientation (tilt) of the swashplate causing a cyclic pitch change to the rotor blades. In a conventional helicopter, gyroscopic precession will cause any cyclic pitch input to be "felt" 90 degrees (or less) after it is input. For a perfectly "rigid" head or a teetering rotor system the precession lag is exactly 90 degrees following the input; for articulated rotor systems the precession is something less than 90 degrees dependent on the rotor flapping offset [Ref. 2]. Similarly, the Hiller paddle experiences the same gyroscopic precession; therefore, the input is applied 90 degrees ahead of where we desire the control deflection to affect the rotor blade pitch. The blade azimuth position, Ψ , is zero over the tail and positive in the direction of rotor rotation [Ref. 2]. In contrast to conventional U.S. helicopters that have a counter-clockwise rotating main rotor system, the main rotor on the Bergen Industrial rotates clockwise. In addition to the Hiller paddles, the rotor blades also experience a 90-degree precession; consequently, for a lateral or longitudinal cyclic attitude change, the actual input is applied 180 degrees ahead of the affected blade position [Ref. 3]. For example, to input a nose down attitude change, the swashplate tilts forward which deflects the paddle at the $\Psi = 90^\circ$ position (negative AOA), the paddle flaps (down) to its minimum low position over the nose, at $\Psi = 180^\circ$, decreasing the rotor pitch on the blade at the $\Psi = 90^\circ$ position. As the blade continues to rotate to the $\Psi = 180^\circ$ position, it reaches its minimum flapping angle (flaps down), forcing the rotor disk to tilt forward causing a nose-down attitude. This nose-down attitude will result in an initial forward acceleration.

C. EQUATIONS OF MOTION

The behavior of the air vehicle in flight can be modeled as a combination of a number of interacting sub-systems (e.g. the fuselage, main rotor, tail rotor, and

empennage). These sub-systems result in the aerodynamic forces and moments about the CG of the body (body axis system). Figure 2.2 shows the orthogonal body axis system used for aircraft dynamic analysis with the associated aerodynamic forces and moments.

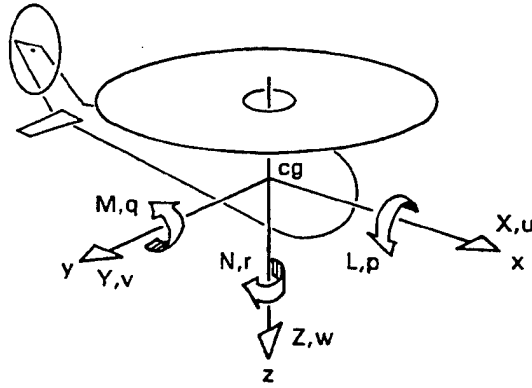


Figure 2.2 Helicopter Orthogonal Axis System [From Ref. 1]

The equations governing these interactions are developed from the application of physical laws, i.e. Newton's laws of motion relating the applied forces and moments to the resulting translational and rotational accelerations [Ref. 1]. Where only the six DOF system is considered, the three translational velocities components are u , v , and w , and the three rotational velocities are p , q and r . The nonlinear equations of motion as presented in Reference 1 are given below.

Force equations

$$\dot{u} = -(wq - vr) + \frac{X}{m} - g \sin \theta \quad (2.1)$$

$$\dot{v} = -(ur - wp) + \frac{Y}{m} + g \cos \theta \sin \phi \quad (2.2)$$

$$\dot{w} = -(vp - uq) + \frac{Z}{m} + q \cos \theta \cos \phi \quad (2.3)$$

Moment equations

$$I_{xx} \dot{p} = (I_{yy} - I_{zz})qr + I_{xz}(\dot{r} + pq) + L \quad (2.4)$$

$$I_{yy} \dot{q} = (I_{zz} - I_{xx})rp + I_{xz}(r^2 - p^2) + M \quad (2.5)$$

$$I_{zz} \dot{r} = (I_{xx} - I_{yy})pq + I_{xz}(\dot{p} - qr) + N \quad (2.6)$$

where the external forces (X , Y , and Z) and moments (L , M , and N) are written as the sum of the contributions from the different aircraft components. I_{xx} , I_{yy} , etc. are the fuselage mass moments about the CG, and m is the aircraft mass. The Euler angles, ϕ , Θ and Ψ , represent the orientation of the fuselage body axis with respect to an earth-fixed coordinate system. The external forces and moments, and Euler angles (save the yaw angle, Ψ) can be written in first order vector form:

$$\frac{d\bar{x}}{dt} = f(\bar{x}, \bar{u}, t) \quad (2.7)$$

where $\mathbf{x}(t)$ is the column vector of state variables, $\mathbf{x}=\{u, w, q, \Theta, v, p, \phi, r\}$ and $\mathbf{u}(t)$ is the vector of control variables. The control vector has four components: longitudinal cyclic, collective, lateral cyclic and pedals (directional control), $\mathbf{u}=\{\delta_e, \delta_c, \delta_a, \delta_p\}$.

D. LINEARIZATION

Using small perturbation theory, we assume that the helicopter behavior can be described as a perturbation from the trim condition. Assuming that the external forces and moments can be represented as analytical functions, we can expand the functions into a Taylor series about an operating point, and retain only the linear terms. The linearized equations of motion for the full six DOF system, describing perturbed motion about a general trim point, can be written as [Ref. 1]:

$$\bar{x}' = A\bar{x} + B\bar{u} \quad (2.8)$$

where A and B are the system and control matrices respectively, derived from the partial derivatives of the nonlinear function, f (alternately referred to as F and G), where

$$A = \left(\frac{df}{dx} \right)_{x=x_e} \quad (2.9)$$

and

$$B = \left(\frac{df}{du} \right)_{x=x_e} \quad (2.10)$$

The elements of the system and control matrices can be found in Appendix A. Note: the linear representation is valid only if the initial angular velocities are zero.

E. STABILITY DERIVATIVES

The elements of the A and B matrices are known as the stability and control derivatives. There are 36 stability derivatives and 24 control derivatives in the standard six DOF system. These derivatives represent the slope of the forces and moments at the trim point reflecting the strict definition of the stability and control derivatives [Ref. 1]. The derivatives are non-dimensionalized by dividing the *change in forces* by the mass of the aircraft, and dividing the *change in moments* about each axis by the appropriate moment of inertia. A complete listing and explanation of all derivatives is presented in References 1 and 2.

F. SOFTWARE (JANRAD)

System identification is the process of constructing a simulation model and associated parameters from experimental data. Numerous system identification programs are available to assist in the UAV “plant” identification process. Many of these programs use a curve fitting process by which experimental data is used to determine the system stability derivatives. To obtain the experimental data necessary to perform these functions requires a fully instrumented air vehicle. The lack of this capability, time requirements, and monetary constraints, led to the use of the JANRAD program to accomplish the task of system identification for the UAV.

The Joint Army/Navy Rotorcraft Analysis and Design (JANRAD) program was developed at NPS as an interactive, MATLAB[®] based program to meet the needs of the aerospace engineering student in preliminary helicopter design [Ref. 4]. The JANRAD program is capable of performing both performance and stability analysis for any rotorcraft. The Performance program, described in the reference, determines the trim solution, and various performance parameters at a given flight condition necessary in the preliminary design. The Stability program calculates the stability derivatives for a given flight condition, and determines the state-space linear model at any trimmable point [Ref.5]. The stability derivatives are determined by using closed-form solutions whenever possible, or by solving multiple trim solutions about a nominal position. For the hover analysis, the stability derivatives from the main and tail rotors have the largest influence on aircraft response.

For the short-term anticipated application requirements of the simulation model, the functional fidelity obtained from the JANRAD linearized model was deemed satisfactory. The JANRAD program was developed for full-scale helicopter design; therefore, the software code required slight modifications to accommodate the parameters representative of a scale-size helicopter model. Output fields were expanded to indicate values representative of the small UAV. Additionally, the output files and plotting routines were changed to allow compatibility with MATLAB upgrades. Continued software enhancements will make the JANRAD program more user-friendly, and increase the software's analysis capabilities [Ref. 6].

G. SIMULATION MODEL

From the study of modern control theory, the NPS student has a working knowledge of the SIMULINK[®] simulation software. Therefore, its use was a natural progression when selecting simulation software. Other programs, such as the Systems

Build (XMATH) programs are available, but require an extensive time investment to become proficient.

The basic SIMULINK Model developed uses state-space analysis of the system discussed above (Equation 2.8). The model is presented in the figure below (Figure 2.3).

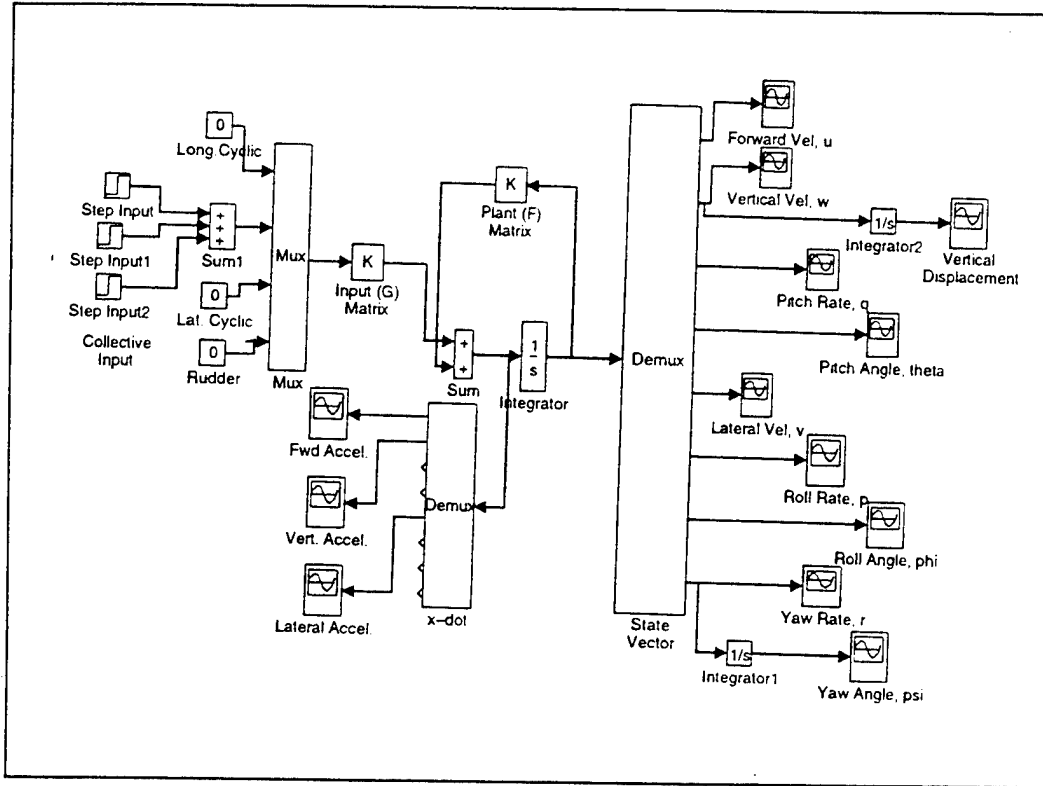


Figure 2.3 Simulink Block Diagram Model

The analysis uses the F & G matrices input about a known trimmable condition. The F&G matrices were computed using the JANRAD *Stability* program. The matrix parameters were entered into a MATLAB[®] file, where the Simulink program was able to read the data. The input vector was designed such that single-channel inputs are possible while holding the remaining controls in the trimmed position. Recall: the control inputs are only changes (i.e. δ_c , δ_e , δ_a or δ_p) from the trimmed condition. The outputs from each element of the state vector are presented with time history plots, such that any output from the state can be analyzed. From the output plots, dynamic response to control input

can be observed in the axis of interest (input), while also observing the cross-coupling effects experienced by the UAV. Information of UAV yaw angle, Ψ , is available by simple integration of the yaw rate, r . Additionally, acceleration data can be observed and later compared with flight test acceleration outputs. Prior to integrating the state-vector to obtain the axial velocities, u , v , *and* w , the state accelerations, \dot{u} , \dot{v} , and \dot{w} , were obtained.

III. INPUT PARAMETERS

The parameters required to conduct the *performance*, and *stability and control* analysis using the JANRAD program were determined either from measurement, table look-up or experimental tests. References (4) and (5) present a full listing of the required input variables. Reference (7) presents scaling as an alternative method to obtain aircraft physical parameters available only by experiment or flight data. The scaling method yields approximate results useful for the initial model development until more accurate means can be employed. A complete listing of all input data is presented in Appendix B.

A. PHYSICAL MEASUREMENTS

Obviously, the most desirable method is that of direct physical measurement. Measurements of those input variables that could be measured from the UAV were taken from an arbitrary reference datum. The datum, located roughly at the unmodified UAV CG, was designated as waterline (WL) zero, and butline (BL) zero. The nose of the helicopter was designated as fuselage station (FS) zero. Additional input data that required "alternative" methods of collection are listed in the following sections.

B. MOMENTS OF INERTIA

When developing a mathematical model for an air vehicle, one cannot overlook the contributions of the aircraft's mass-moments of inertia to its controllability and dynamic responses. The mass-moments of inertia represent the vehicle's resistance to acceleration or rotation given a control input or external perturbation. Direct calculations of the moments of inertia can be accomplished by multiplying the mass of each component by the square of the distance to the body axis of rotation. For the scale UAV, this method is impractical because the air vehicle's individual parts are too small and light to yield anywhere near accurate results [Ref. 7]. Therefore, the aircraft's moments of inertia must be determined by experimental methods. The reference describes two methods of developing a compound pendulum for obtaining the necessary moments experimentally.

the overhead pivot and the pivot at CG. The overhead pivot method of the compound pendulum was utilized.

By suspending the UAV with small wires to a single pivot point on the ceiling, we can develop a compound pendulum (system). Knowing the vehicle mass, m , and distance, d , from the UAV CG to the pivot point, we can determine the moment of inertia about the helicopter's CG, I_{CG} , using the parallel axis relation:

$$I = I_{CG} + md^2 \quad (3.1)$$

By giving the UAV a gentle push in a particular direction (along a body axis), we can oscillate the system, exciting the rotation of the body. The oscillatory period is determined by counting the number of cycles for a particular elapsed time. A cycle is defined as one complete oscillation to and fro. The period of the system will be dependent upon the body's moment, I_{CG} , the distance to the point of rotation, d , and the mass, m . The oscillatory period, p_{M+S} , is simply the total elapsed time (in seconds) divided by the total number of cycles. Reference 7 provides the equation for calculating I_{CG} of the oscillating model:

$$I_{CG} = Wl \left[\frac{p_{M+S}^2}{4\pi^2} - \frac{l}{g} \right] - I_0 \quad (3.2)$$

where W is the weight of the model, l is the distance from the pivot to the body C.G., and I_0 is the moment contribution of the supporting structure. To obtain the desired moments about all three body axes, the model was hung three different ways in order to obtain rotation about the axis of interest. Initially the tests were conducted using chains to mount the model to the ceiling. The results were suspect most likely due to the weight of the chain dominating the calculations leading to results, $-1 < I_{CG} < 1$ [slug-ft²]. Therefore, to eliminate the influence of the supporting structure, the experiment was repeated using lightweight, monofilament fishing line (I_0 assumed zero when using light-weight wire

supports). The results of Trial 2 show that the moment about the x-axis and y-axis are the same. Since there was limited rotational motion about the axis of interest by displacing the system only a small amount, the system reacted similar to a point mass confirming these results.

The experiment was conducted yet again (Trial 3) with a shorter distance from the UAV CG to the pivot point. This was done to further excite the rotational motion about the axis of concern. The results from this trial more closely match the values calculated from the scaling method (with a scaling factor, $\lambda=10.6$). A complete listing of the experimentally determined mass-moments of inertia are presented below (Table 3.1). The experimental specifications and resulting calculations are presented in Appendix C.

Trial	I_{xx} [slug-ft ²]	I_{yy} [slug-ft ²]	I_{zz} [slug-ft ²]
Scaling	.0374	.2989	.2615
1	.876	1.32	(.93)
2	.658	.658	1.887
3	.0709	.3967	-----

Table 3.1 Moment of Inertia Results

C. ROTOR FLAPPING MOMENT

The rotor flapping moment is the mass-moment of inertia of the blade about the flapping hinge. The rotor flapping moment influences the rotor blade's ability to flap due to blade pitch changes caused by cyclic inputs. The moment of inertia is defined as [Ref.2]:

$$I = \int_0^R mr^2 dr \text{ [slug-ft}^2\text{]} \quad (3.3)$$

where m is the specific mass of the blade (slug/ft), r is the radius of the blade element, and R is the total blade radius. For the main and tail rotors, the blade mass distribution was assumed uniform; therefore, the above relation can be simplified:

$$I = mR^2/3 \quad [\text{slug-ft}^2] \quad (3.4)$$

where in this relation, m is the total blade mass (slugs). The results of these calculations are shown below.

$$I_{\text{MRf}} = .034 \quad [\text{slug-ft}^2] \quad I_{\text{TRf}} = 2.8 \times 10^{-5} \quad [\text{slug-ft}^2]$$

D. EFFECTIVE HINGE OFFSET

To eliminate the rolling moment characteristic of the early autogyro and rotorcraft using rigid blades, the blade was allowed to flap about a flapping hinge. For rigid rotor systems, this flapping is accomplished by substituting a flexible section next to the hub [Ref. 2]. The hinge offset of a fully articulated rotor system is merely the radial distance from the rotor hub to the rotor-flapping hinge. For a rigid rotor system, such as that used on the Bergen UAV, an *effective* hinge offset must be determined. The effective hinge offset is dependent upon the main rotor blade's natural frequency, and rotor rotational velocity. The natural frequency of the blade is dependent upon the blade stiffness, blade length and mass. The stiffness coefficient of the blade is not a parameter normally specified in a RC helicopter owner's manual; therefore, it must be determined experimentally. The basis of the experimental determination of the stiffness coefficient, EI , of the blade is that the deflection, v_{MAX} , of a cantilever beam subjected to a point load, P , as illustrated in Figure 3.1, is inversely proportional to EI .

This relationship is provided in Reference 8 by the equation:

$$v_{\text{MAX}} = PL^3/3EI \quad (3.5)$$

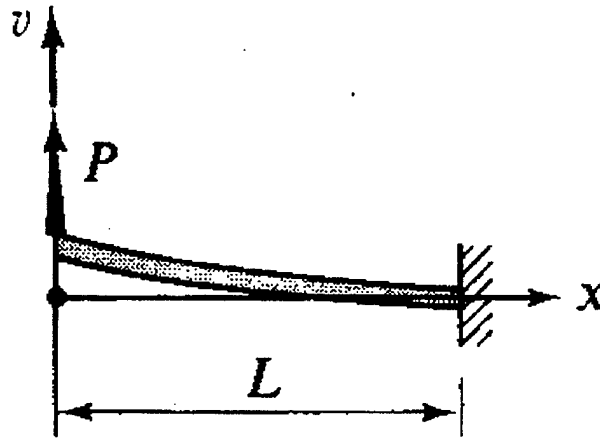


Figure 3.1 Deflection of Cantilever Beam to a Point Load [From Ref. 8]

where L is the beam length. To simplify the calculations, the blade was assumed homogeneous, and of constant cross section. The blade was placed in a vice, and using a fish scale, various loads were applied at the tip of the blade, and the deflections were recorded. Additionally a second method was performed where the tip was deflected a particular distance, and the applied load measured.

The experimental data is plotted below (Figure 3.2) with calculations and results presented in Appendix D. With the blade stiffness coefficient determined, we can now calculate the natural frequency of the blade, ω_1 . Reference 9 provides the required relation:

$$\omega_1 = 3.515 \sqrt{EI/mL^3} \quad (3.6)$$

where ω_1 is the natural frequency for the first bending mode of the blade, and m is the mass of the blade.

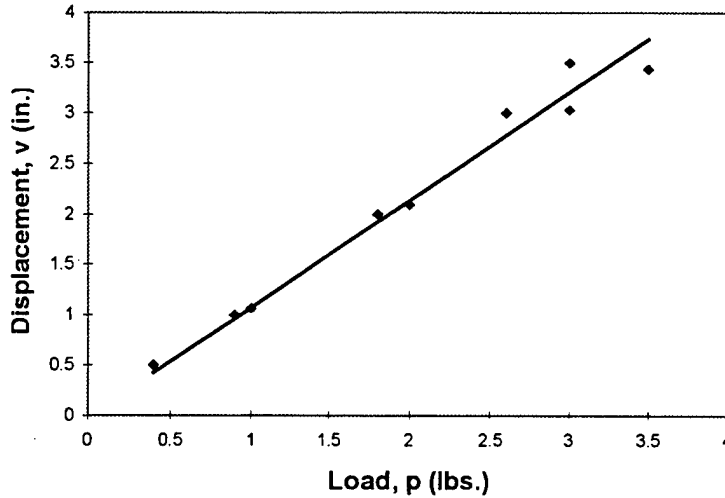


Figure 3.2 Plot of Beam Deflection vs. Applied Load

From the blade natural frequency and the rotational frequency of the main rotor, Ω , we can determine the effective hinge offset ratio from the equation provided by Reference 2 (pg. 457):

$$\left(\frac{e}{R}\right)_{\text{eff}} = \frac{2\left[\left(\frac{\omega_n}{\Omega}\right)^2 - 1\right]}{1 + 2\left(\frac{\omega_n}{\Omega}\right)^2} \quad (3.7)$$

From this analysis, the frequency ratio, $\omega_n/\Omega < 0$ leads to a value of $(e/R)_{\text{eff}} < 0$. The physical implications would be that the rotor system exhibits no effective hinge offset. As was described in Chapter 2, the Hiller paddles drive the cyclic pitch of the rotor blades, and are free to flap about the rotor head. The Hiller paddles essentially operate the same as a teetering rotor system which has a hinge offset of zero [Ref. 2]. With a hinge offset of zero, the rotor flapping response is exactly 90° out of phase with the applied cyclic pitch. Which agrees with the basic design of the UAV cyclic control phase relationship where the

swashplate input is exactly 90° out of phase with the desired disk movement (from the action of the Hiller flybar).

E. AERODYNAMIC INPUTS

Several of the required input data for the JANRAD program were neither available by direct measurement nor experimentally; therefore, several resources were required to satisfy the required data input fields. Many of these data were aerodynamic coefficients of control surfaces, or pressure ratios experienced by these aerodynamic surfaces used in the performance analysis. Below is a listing of these input data with a brief description, reasoning and reference source.

Flight Conditions: Required input data concerning the flight conditions were input as a standard flight test day of 60 degrees Fahrenheit and pressure altitude of 100 ft MSL. For comparison with actual flight data, flight condition information is available from the local airport weather center.

Forward Velocity: For the hover analysis, forward velocity is equal to zero (no wind condition). If performing an analysis of forward flight, UAV airspeed data is required in order to conduct an accurate simulation analysis. At present, this capability does not exist from the vehicle, however, a simple method can be devised by determining the time to fly between two points a known distance apart yielding an approximate, no wind, velocity. Future sensor enhancements may incorporate an internal capability. Note: the JANRAD analysis does not recognize *forward* airspeeds below 12 knots, and accuracy is limited below 50 knots [Ref. 4].

Fuselage Downwash Ratio (due to rotor): The fuselage downwash ratio corrects for the interference of the fuselage due to the downwash of the main rotor system. Using the analysis in Reference 2 (Figure 8.11 pg. 494) with $X'/R = -1.07$ and $Z'/R = +0.19$, an approximate value of v_H/v_1 of 1.5 was selected.

Main and Tail Rotor Lift Curve Slope: Exact airfoil data for the Bergen UAV was unavailable from the manufacturer, and time constraints limited windtunnel

testing. References 2 and 10 provide example lift curve slope values for helicopter rotor blades. From the values presented, a typical value of 5.73 (per radian) was used for the analysis.

Rotor Rotational Velocity: The rotational velocity of the main rotor system was determined using a RPM checker. With the UAV hovering at its operational rotation velocity, the rotational velocity was collected in rotations per minute (RPM). These values were verified during the flight tests by analysis of the vibration data. The rotational velocity of the tail rotor was determined by using the gearing ratio between the main rotor and the tail rotor (1: 4.6). The throttle controller on the UAV is not a constant RPM system, i.e. as rotor loads increase, the rotor rotational velocity increases. Limited data was collected during initial flight-testing; therefore, the operating RPM should be verified during each flight prior to performing the computer simulation.

Rotor Blade Airfoil: As stated above, the UAV airfoil data was unavailable. An additional limitation on the analysis performed is that the JANRAD software used contains only data for three airfoil models: NACA 0012, Boeing VR-12 and the HH-02 [Ref. 5]. The main rotor has a cambered airfoil; therefore, the analysis was performed using a cambered airfoil. The VR-12 was selected.

Horizontal and Vertical Tail Coefficients of Lift and Drag: Both the horizontal and vertical tails are flat plates. Airfoil data for these surfaces is available in References 2, 11 and 12. For a flat plate airfoil, a value of the maximum lift coefficient, C_{lmax} , equal to 0.8 can be expected [Ref. 2]. The coefficient of drag, C_d , for a flat plate is between 0.004 and 0.006 [Ref. 12]; a value of 0.005 was used.

Horizontal and Vertical Tail Lift Curve Slope: The expected values of the empennage surface lift curve slope are dependent upon the airfoil sections and their aspect ratios [Ref. 2]. For the flat plate, representative values are plotted against effective aspect ratio, AR_e . Using the AR_e of the horizontal surface, the value of $dC_l/d\alpha$ was obtained.

Dynamic Pressure Ratio: The dynamic pressure ratio, q_H/q , provides for a corrected flight condition (dynamic pressure) experienced by the empennage due to the

presence of the main rotor system (rotor wake). From the curves provided in Reference 2, an approximate value of 0.6 was obtained.

Rotor Downwash Ratio: The rotor downwash ratio, v_H/v_I , is a ratio of vertical velocities where v_H is the vertical velocity at the horizontal stabilizer, and v_I is the vertical velocity of the induced velocity in the plane of the rotor. This ratio is dependent upon the horizontal and vertical position of the stabilizer with respect to the rotor hub. From the data curves provided in Reference 2, a representative value of 1.5 was used.

Fuselage Downwash Ratio: The fuselage downwash ratio gives the coefficient of the downwash effect of the fuselage on the horizontal stabilizer. Reference 2 provides coefficient values for use as an input parameter for helicopters with or without wings. The original UAV configuration has no wing; therefore, the value of $d\varepsilon_F/d\alpha_F$ selected was 0.06.

F. CONTROL RIGGING DIAGRAMS

To determine the required data for computing the control derivatives, the UAV control-rigging scheme was needed. For the sample helicopter used in Reference 2, the rigging charts are plotted with degrees of rotor blade pitch, either A_1 or B_1 for cyclic inputs, versus inches of cyclic stick deflection. Because the UAV is controlled remotely using radio inputs, or pulse width modulation (PWM), it was desired to plot control surface movement versus PWM. Using this methodology, we can determine the applied control input by comparing the "captured" PWM signal sent to the UAV during a certain maneuver, then model the input and response for comparison with flight data.

The rigging data was collected separately from each of the four inputs: longitudinal cyclic, collective (throttle), lateral cyclic, and directional pedals. For each measurement taken, the helicopter and flybar were leveled both longitudinally and laterally using a bubble-sight level. Using the Schluter AOA Gauge (Figure 3.3), we were able to measure

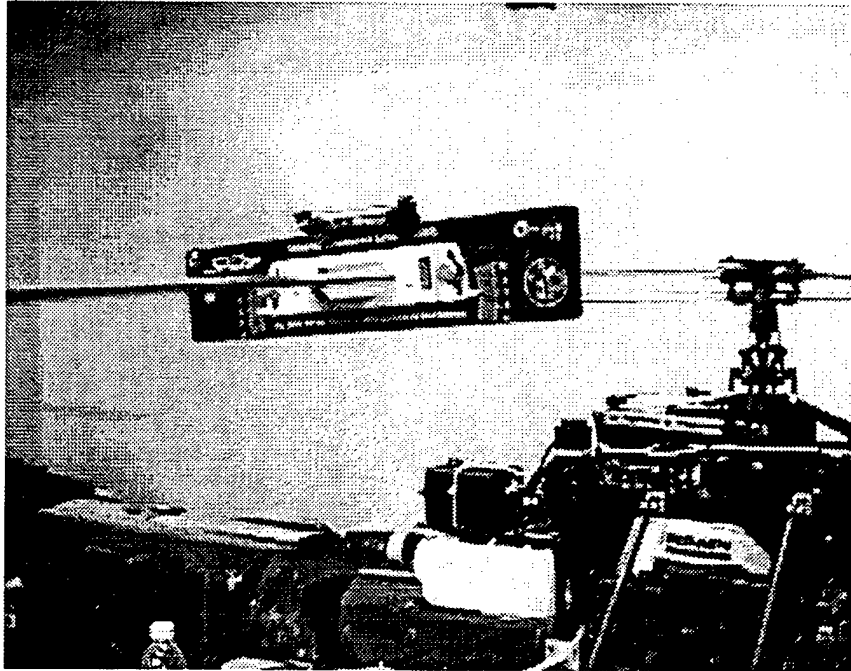


Figure 3.3 Schluter Blade Angle Measurement Device

rotor blade AOA while the corresponding PWM signal required to maintain that control position was collected (at the ground station). For longitudinal cyclic, and collective pitch, blade AOA was measured with the blade at $\Psi = 90^\circ$ (90° ahead of desired reaction due to gyroscopic precession). Lateral cyclic data was collected with the rotor at the $\Psi = 180^\circ$ position. When taking AOA measurements in both cyclic channels, it was necessary to apply PWM *collective* control to bring the neutral cyclic pitch to 0° AOA. Figures 3.4 through 3.7 show the experimentally collected data. A trendline was used to determine the slope of the data for input to the control matrix and compensate for measurement errors. During the simulation run, the control inputs applied will be with respect to PWM signal rather than inches of control stick deflection.

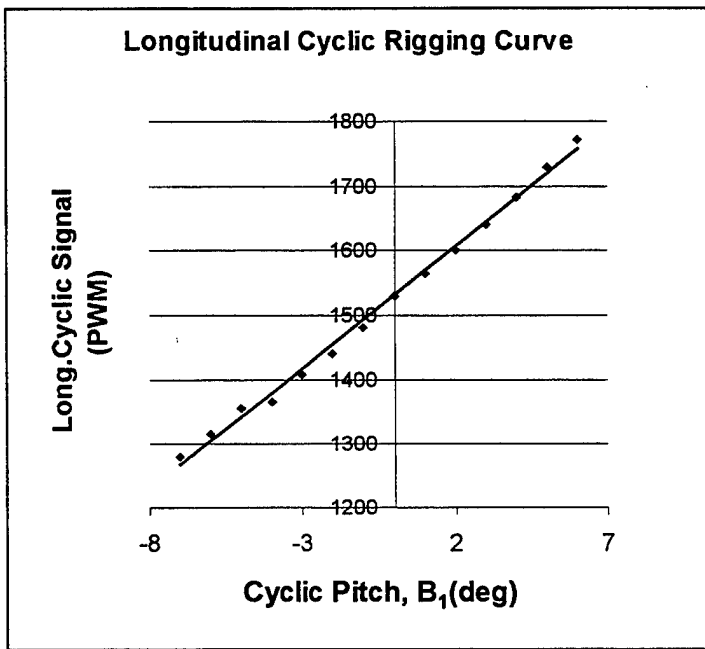


Figure 3.4 Longitudinal Cyclic Rigging Curve

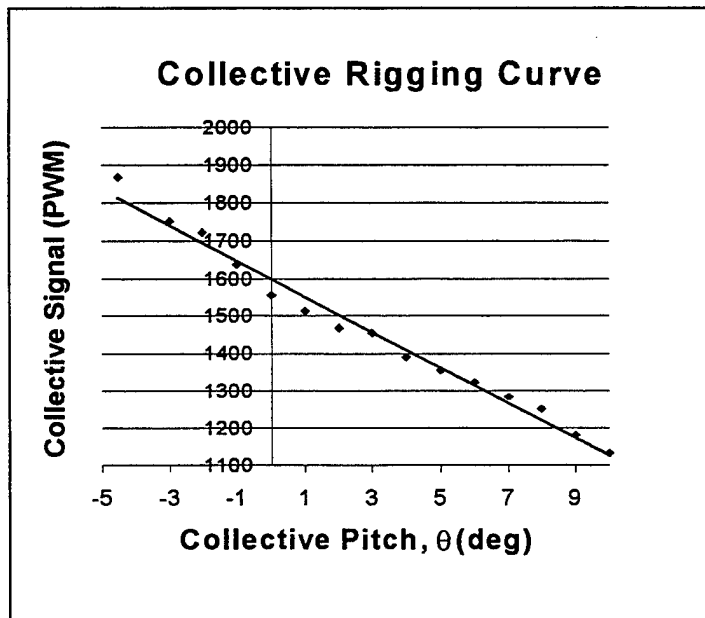


Figure 3.5 Collective Rigging Curve

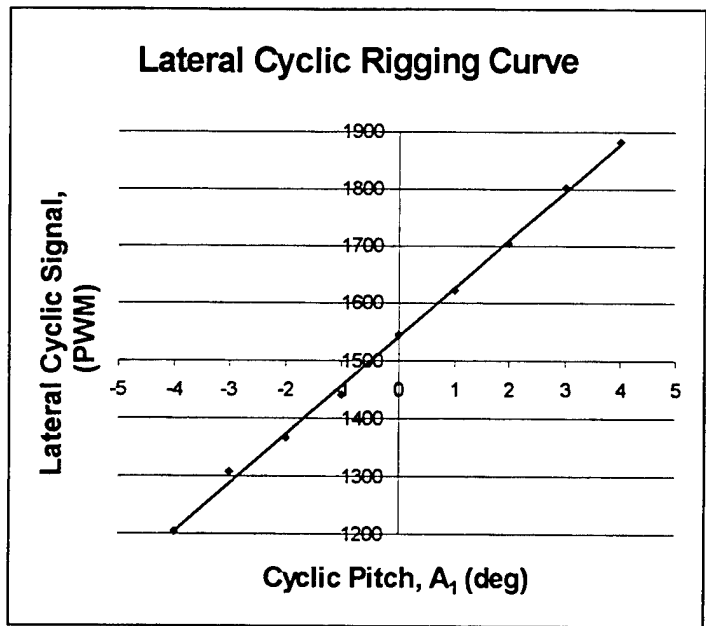


Figure 3.6 Lateral Cyclic Rigging Curve

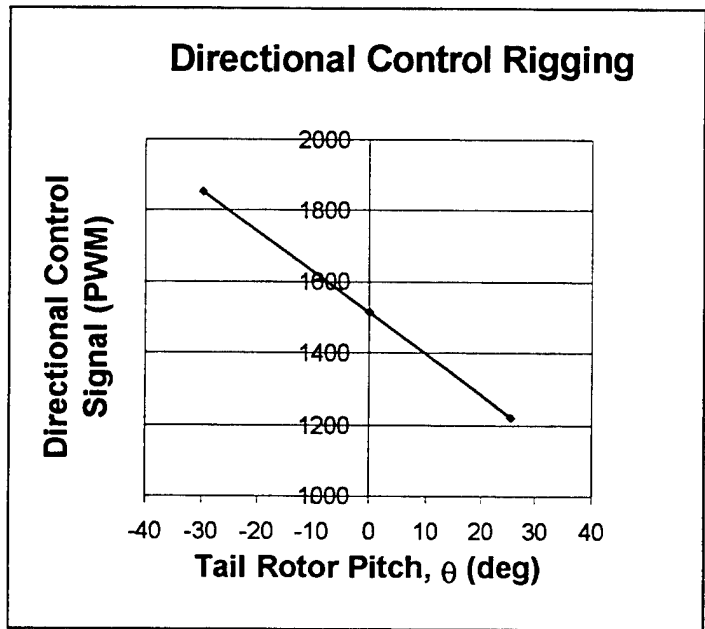


Figure 3.7 Directional Control Rigging Curve

IV. SIMULATION ANALYSIS

A. JANRAD IN HOVER

The first step in the analysis of our model is the use of the JANRAD *Performance* program to evaluate the UAV trim condition. Once the helicopter trim position is determined, the trim solution can then be used to evaluate certain performance parameters. The JANRAD program was developed as a preliminary design tool, and uses the harmonic balance method to trim the rotor using actual 2D airfoil data. The procedures for running the original JANRAD program are outlined in Reference 4. The enhanced JANRAD 98 version is also available with increased capabilities and a user-friendly Graphical User Interface (GUI) [Ref. 6].

1. Performance Calculations

The analysis was conducted using the input data developed in Chapter 3 with a complete listing in Appendix B. The results of the Performance analysis are listed below (Table 4.1) in the output format from JANRAD. Many of the values are zero with the UAV in a hover.

Fuselage drag = 0.00 lbs.	1st long cyclic term-B1 (deg) = 0.00
Rotor drag = 0.00 lbs.	Solidity (sigma) = 0.045
Wing lift = 0 lbs.	Disk loading = 0.78 lbs/ft ²
Wing drag = 0 lbs.	Figure of Merit = 0.46
Horizontal tail lift = 0.00 lbs.	CT/sigma = 0.034
Horizontal tail drag = 0.00 lbs.	CQ/sigma = 0.0021
Vertical tail side force = 0.00 lbs.	CH/sigma = 0.0000
Vertical tail drag = 0.00 lbs.	Tip mach of the adv. blade = 0.415
Tip path angle = 0.00 degs	Advance ratio = 0.000
Rotor coning angle = 1.58 degs	Rotor thrust required (TPP) = 19.67 lbs.
Location of mean thrust (r/R) = 0.75	Rotor power required = 1.01 h.p.
Collective pitch at .7 r/R = 4.61 degs	Rotor torque = 3.37 ft-lbs.
1st lat cyclic term-A1 (deg) = 0.00	

Table 4.1 Listing of JANRAD Performance Output Data

Verification of the JANRAD calculations is only possible by generic computations from Reference 2. Testing equipment is also not available for comparison or verification. The trim solution determined in the *Performance* program is also used as a starting point for the *Stability Analysis* program.

2. Stability Analysis

The JANRAD *Stability Analysis* Program [Ref. 5] provides the stability and control derivatives (F and G matrices) which become the plant of our simulation model. The calculated matrices are listed in Appendix E. These matrices can also be used to perform an open-loop stability analysis by analyzing the open loop eigenvalues, and performing a frequency response analysis or “Bode Diagram”.

For small amplitude stability analysis, helicopter motion can be considered to comprise a linear combination of natural modes, each having its own unique frequency, damping and distribution of the response variables [Ref. 1]. Using the stability matrix, F (or A), we can describe the free motion of the UAV in the form:

$$\dot{x} - Ax = 0 \quad (4.1)$$

subject to the initial conditions, $x(0)=x_0$. The natural modes are described as linearly independent so that no single mode can be made up of a linear combination of the others. Then, if a single mode is excited, we should expect the motion to remain in that mode only. In the table below (Table 4.2), we provide a listing of the system eigenvalues, which are also plotted in Figure 4.1. From the complete list of eigenvalues, we can decouple the system in order to separate the eigenvalues into two sets, the longitudinal and the lateral modes. The characteristic roots, which appear as complex conjugate pairs, represent an oscillatory response for that mode.

<i>Eigenvalues</i>	<i>Freq. (rad/sec)</i>	<i>Damping</i>
-5.2075	5.2075	1.00
-1.8853	1.8853	1.00
-0.7560	0.7560	1.00
-0.6625	0.6625	1.00
0.2149+0.5811i	0.6196	-0.3469
0.2149-0.5811i	0.6196	-0.3469
0.1890+0.4094i	0.4510	-0.4191
0.1890-0.4094i	0.4510	-0.4191

Table 4.2 Eigenvalues of the Linearized Model

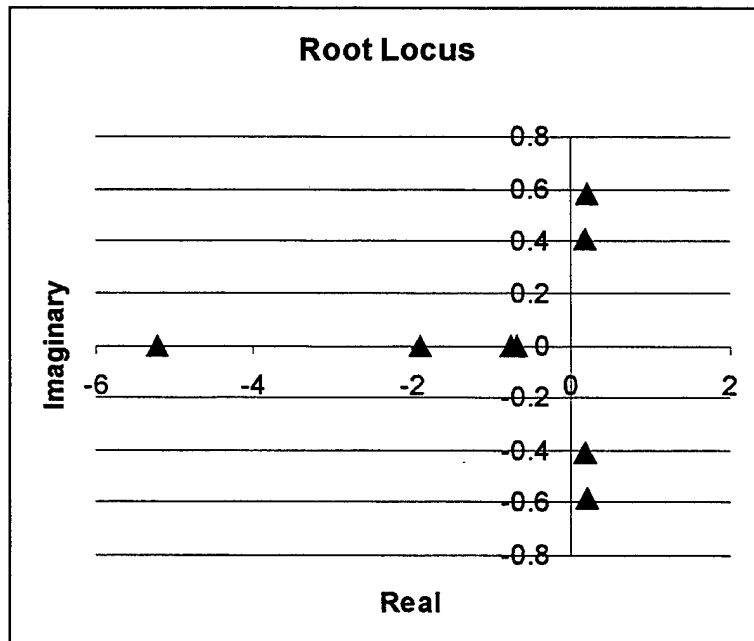


Figure 4.1 Open-Loop Eigenvalue Plot

The stability of the UAV can be discussed in terms of the individual eigenvalues, which is determined by the sign of the real part of the root. A root with a negative real part, or located on the left-hand side of the argon plane is stable, while a root with a positive real part (right-hand side of plane) is unstable.

We can see there exists two unstable, oscillatory roots. The first pair:

$$\lambda=0.1890 \pm 0.4094i$$

correspond to the longitudinal phugoid, or long period, mode. This mode also has a negative damping value which can lead to a divergent longitudinal mode when excited. The long period ($P=13.93$ seconds) characteristic of this mode can be easily controlled by a pilot in the loop, or automatic flight control system. The second pair of unstable, oscillatory roots:

$$\lambda=0.2149 \pm 0.5811i$$

correspond to the lateral dutch roll mode. This mode has a period of 10.14 seconds, and again could be pilot or stability augmentation system controlled. For the open loop simulation analysis, these instabilities may prove problematic.

An additional method for analyzing the relative stability of a system is by the use of frequency-response tests. By the term frequency-response, we are referring to the steady-state response of the system to a sinusoidal input. Using this method, we vary the frequency of the input to the system over a certain range and study the resulting system response. A complete frequency-response analysis would include the response of each state of the system to all the possible inputs. For the helicopter, this would involve analyzing the eight states of the system to each of the four possible inputs. At this point, we are not concerned with the effects of cross-coupling (off-axis response to control input); therefore, we will concern ourselves with looking at the responses along the three orthogonal axes from inputs along those same axes (i.e. vertical response to a vertical, or collective, input, etc.). The frequency-response analysis is graphically depicted by either the Nyquist Plot or the Bode Diagram. To plot system response magnitudes, the Bode

diagram uses a semi-logarithmic plot of system response in decibels, dB, plotted against input frequency in radians. A second plot shows the system phase angle -- the angular difference between the harmonic input and the system response. One important characteristic we can determine from the Bode plot is the "bandwidth". The bandwidth is indicated by the frequency at which the response has decreased by 3 dB, or about 71 percent of the initial response.

By applying any control input, we can determine the frequency-response to the mathematical model by using the MATLAB command "bode (F, G, C, D, iu)", where F , G , C and D are the matrices of the state-space model, and iu produces an input to the i th element of the control input vector. Figure 4.2 provides the Bode plot for a longitudinal response (forward velocity, u) to a *longitudinal* cyclic input, δ_e . The effective bandwidth for the longitudinal cyclic is approximately 0.50 rad/sec. From the lower plot, we note that the system displays a phase "lead". This is characteristic of systems with an unstable root in a particular channel. Figure 4.3 is the result of applying a *collective* input to the model, and analyzing the frequency-response in the vertical axis. The bandwidth for this input is approximately 1.5 rad/sec with a phase "lag" as indicated by the lower plot. Applying a *lateral* input to the system (Figure 4.4), and looking at the frequency-response in the lateral axis yields similar results as seen in the first plot (Figure 4.2). The gain drops 3 dB at a frequency of approximately 0.70 rad/sec. The phase shift again is shown to be unstable.

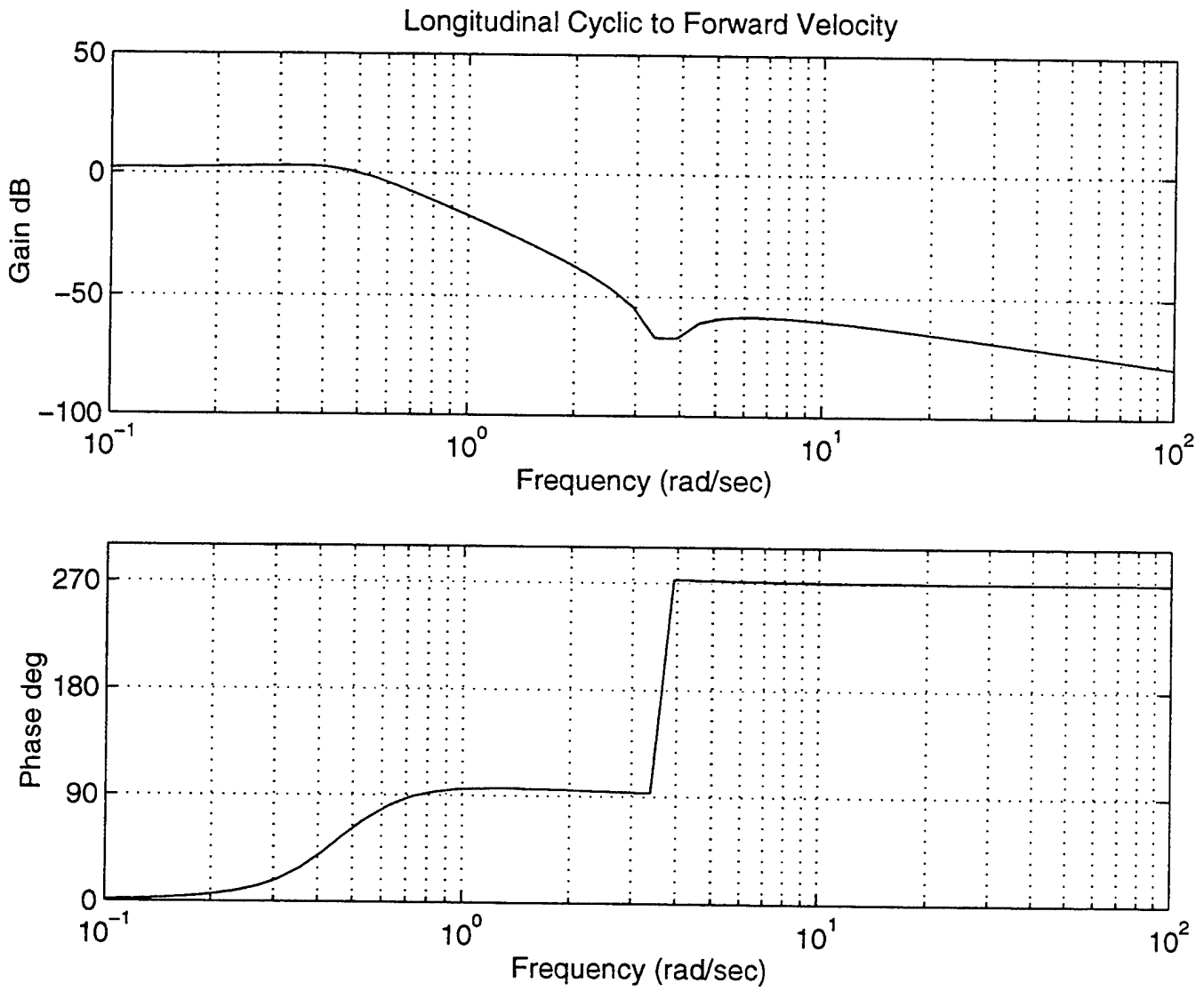


Figure 4.2 Bode Plot of Longitudinal Cyclic to Forward Velocity

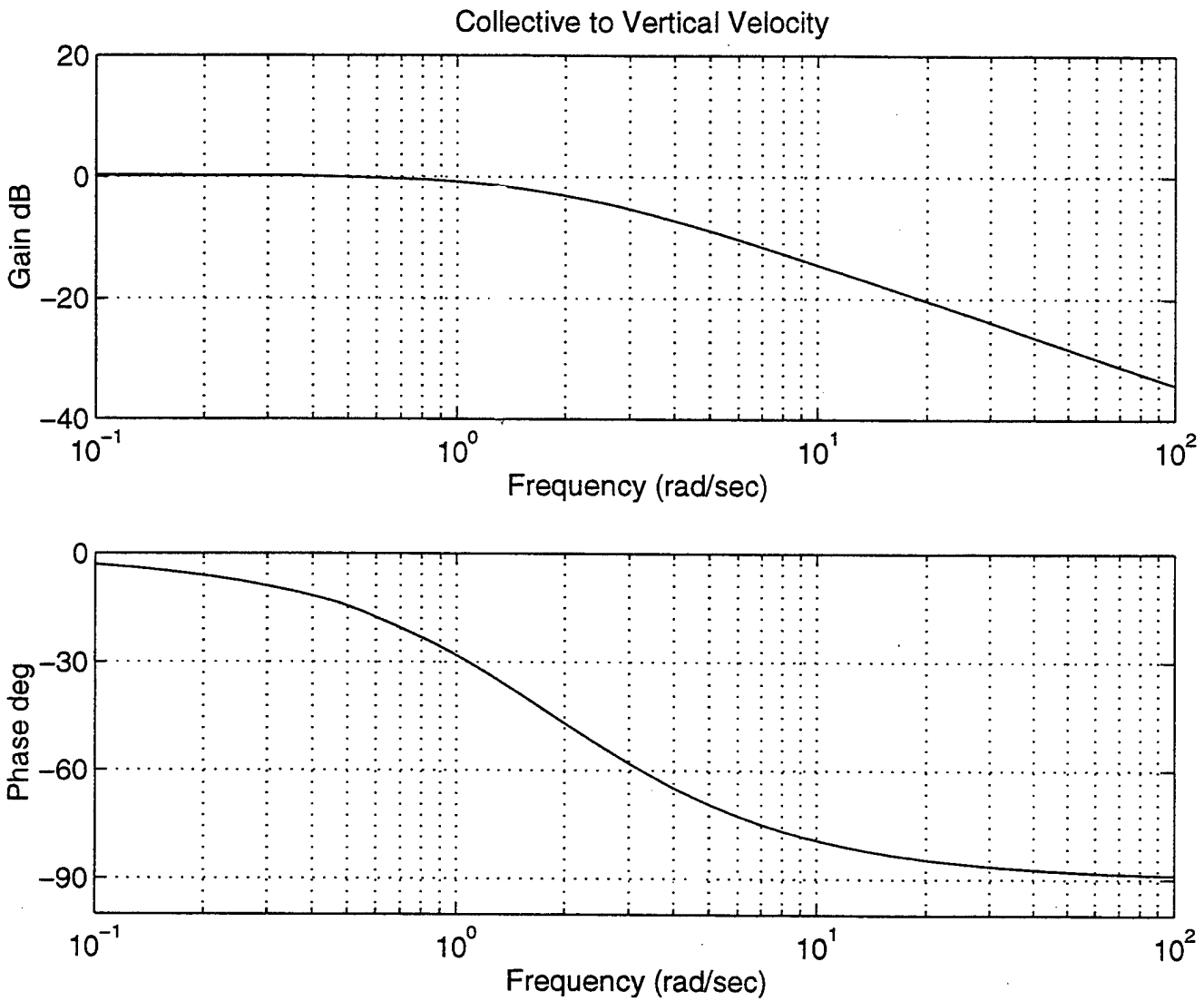


Figure 4.3 Bode Plot of Collective to Vertical Velocity

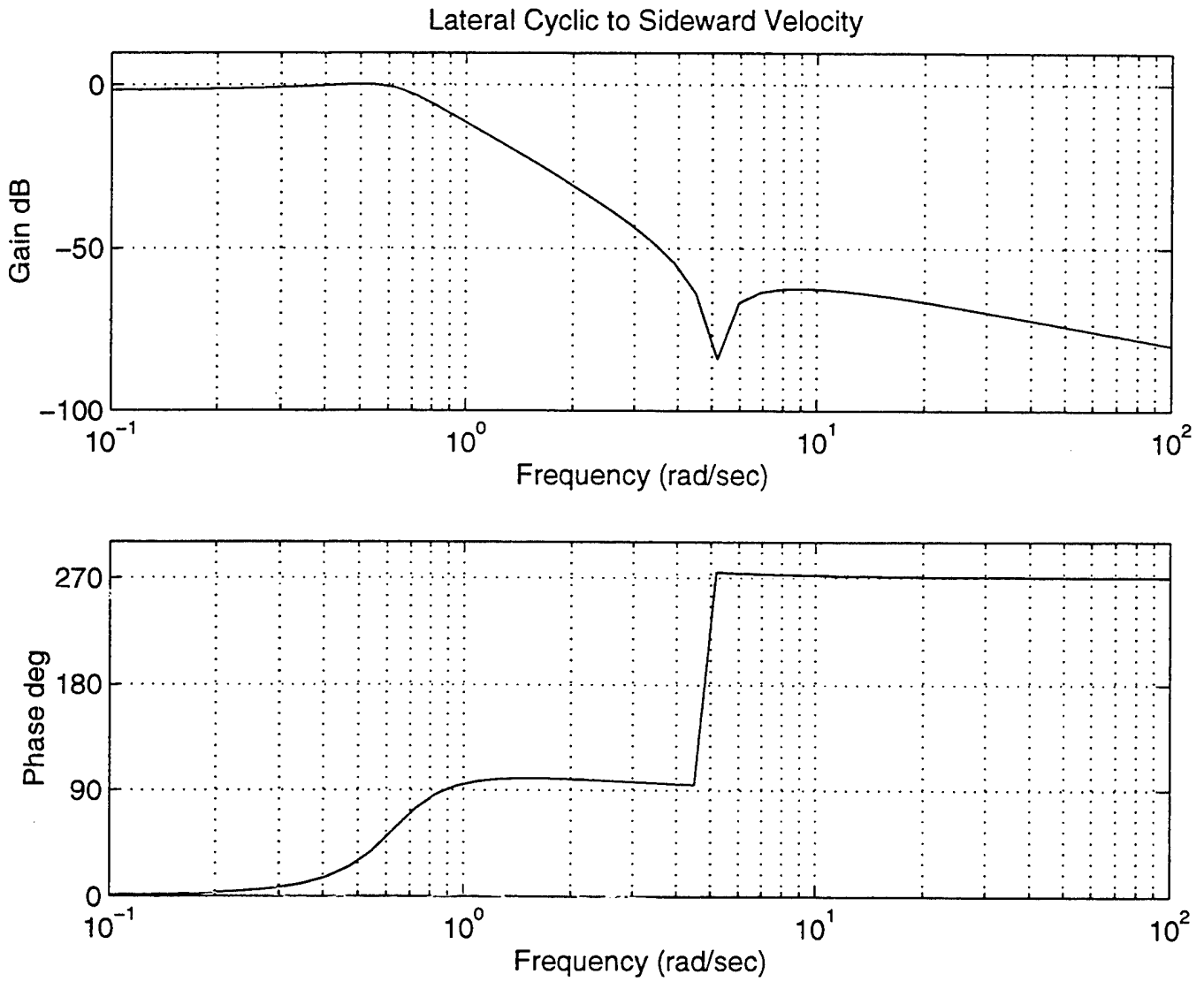


Figure 4.4 Bode Plot of Lateral Cyclic to Sideward Velocity

B. SIMULINK MODEL IN HOVER

The above analysis provides some insight to the inherent *stability* of the simulation model by using the frequency-domain method. By applying discrete inputs to our simulation model, we can analyze the responses in the *time* domain.

Using our Simulink model developed in Chapter 3, we can input either a unit step, impulse or doublet to perturb the model from its trim condition, and examine any or all of the eight “states” of the system. As was done in the previous section, our initial analysis of the system will be primarily restricted to analyzing the response along the axis of the applied input. Recall when we plotted control rigging schedules for the four UAV inputs, each was plotted versus the radio controller signal, or PWM, required to maintain the control position. Therefore, to apply a realistic input to the simulation model, the magnitude of the input signal was adjusted to change the control surface by approximately one degree (either cyclically or collectively). Small inputs were used in an effort to predict the actual UAV responses (displacements) anticipated during testing to remain within the flight-test operating area. The following time-history simulations show both short-term initial UAV responses, as well as “long-term” oscillations.

Figure 4.5 shows the applied longitudinal doublet input and the resulting forward acceleration, velocity, and pitch angle response. Recall from the stability analysis that the longitudinal phugoid mode was unstable, causing extreme divergent oscillations as time progresses. Of particular interest is the period of the phugoid oscillations; from the figure, we can see an oscillation period of approximately 14 seconds which matches our earlier analysis of the characteristic roots. Because of the large scale along the acceleration vertical axis, it is difficult to discern the magnitude of the initial acceleration response; therefore, the simulation was replotted showing the initial, short-term response (Figure 4.6). The initial longitudinal acceleration shows an acceleration of only 0.1 G's.

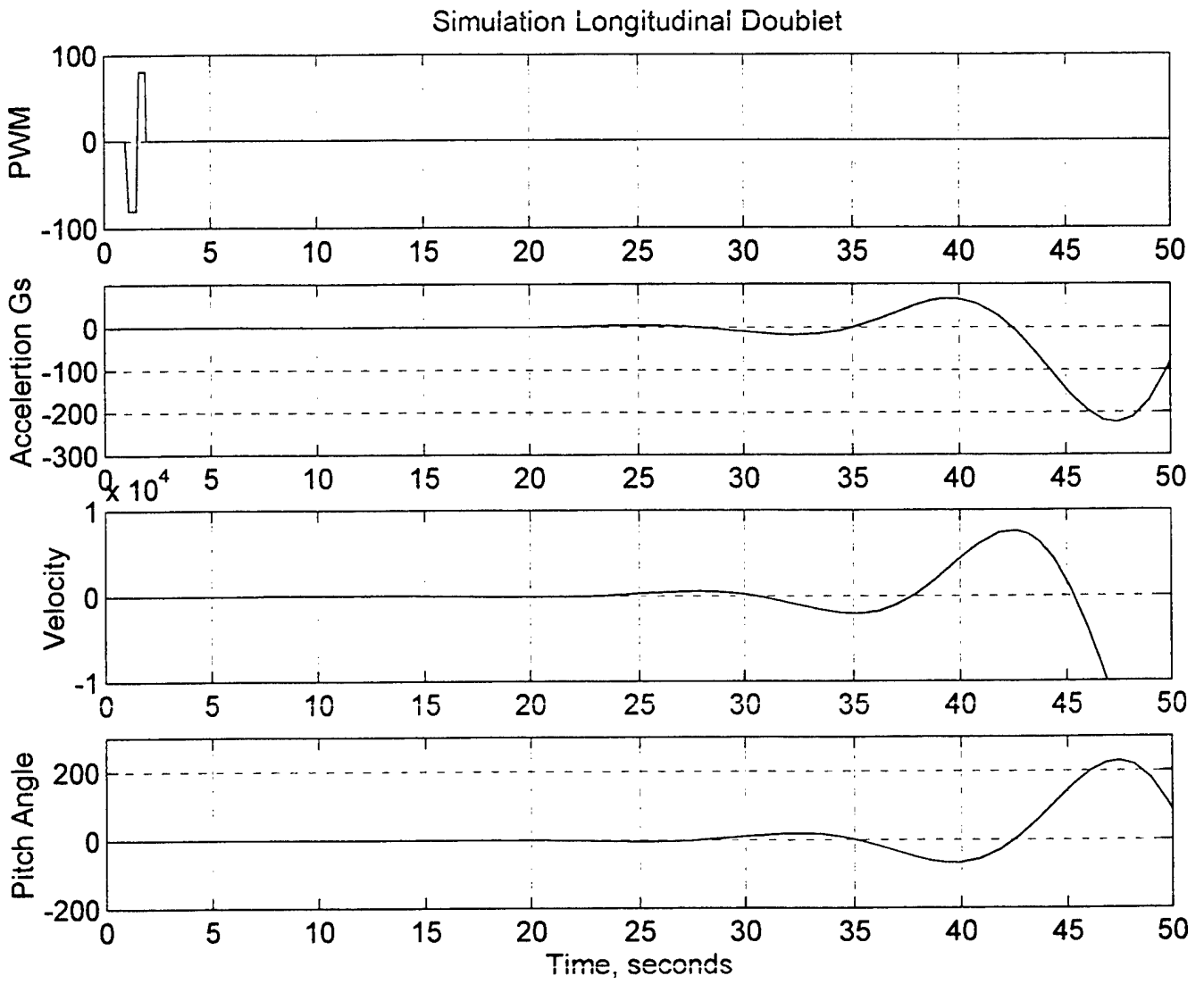


Figure 4.5 Long-Term Longitudinal Doublet Simulation

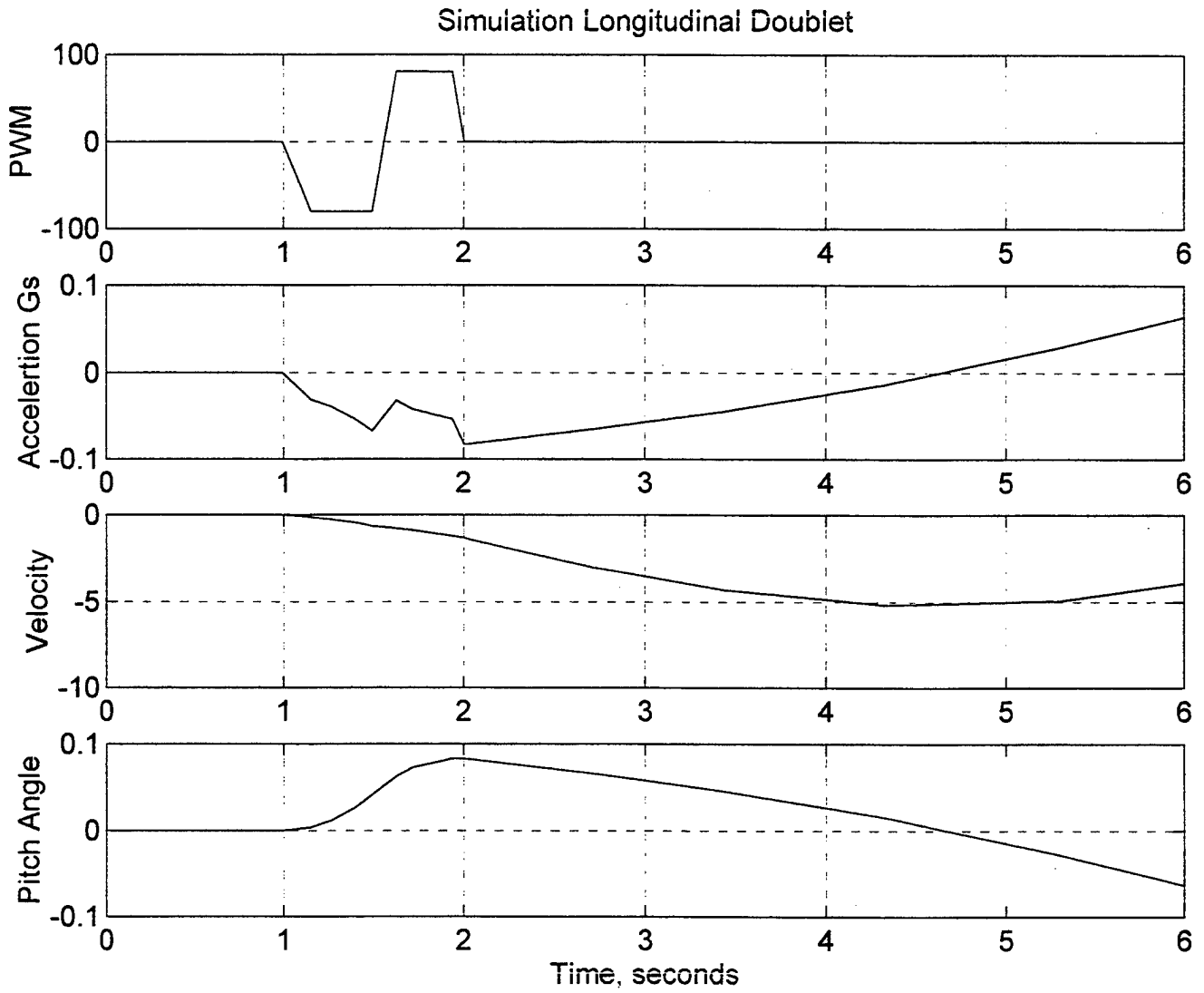


Figure 4.6 Short-Term Longitudinal Doublet Simulation

A similar input was applied to the vertical axis by applying a collective doublet to the simulation model, and plotting the acceleration and yaw angle, Ψ . Figure 4.7 indicates the model responded as expected; the model accelerates up and down following the collective inputs, then, because the system is stable in the vertical channel, returns to the trim position. The model yaws in response to the collective input, and also returns to the trim condition. At approximately 10 seconds in the simulation, the yaw angle starts to deviate once again in response to coupling instabilities in the other axes.

For the lateral mode, a lateral (cyclic) impulse was applied; the impulse and doublet are both useful in exciting the long-period instabilities of the system. The resulting simulation is shown in Figure 4.8. Similar to Figure 4.5 above, the system eventually goes divergent due to the unstable dutch-roll characteristic root. The period of this unstable root from above was calculated to be approximately 10 seconds, which is depicted in the resulting acceleration, velocity and roll angle shown in the figure. The short-term response (Figure 4.9) indicates an initial lateral acceleration of approximately 0.2 G's.

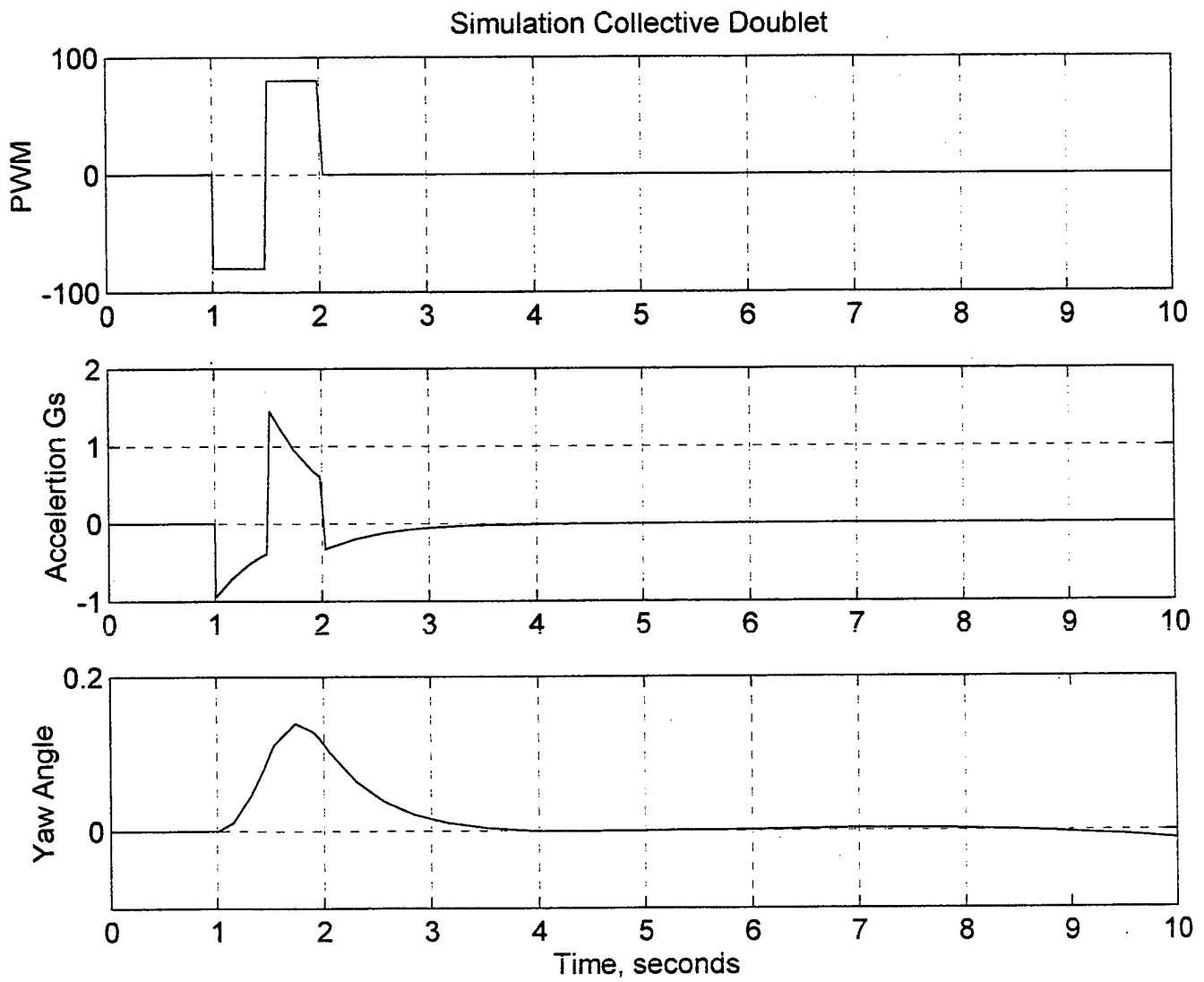


Figure 4.7 Collective Doublet Simulation

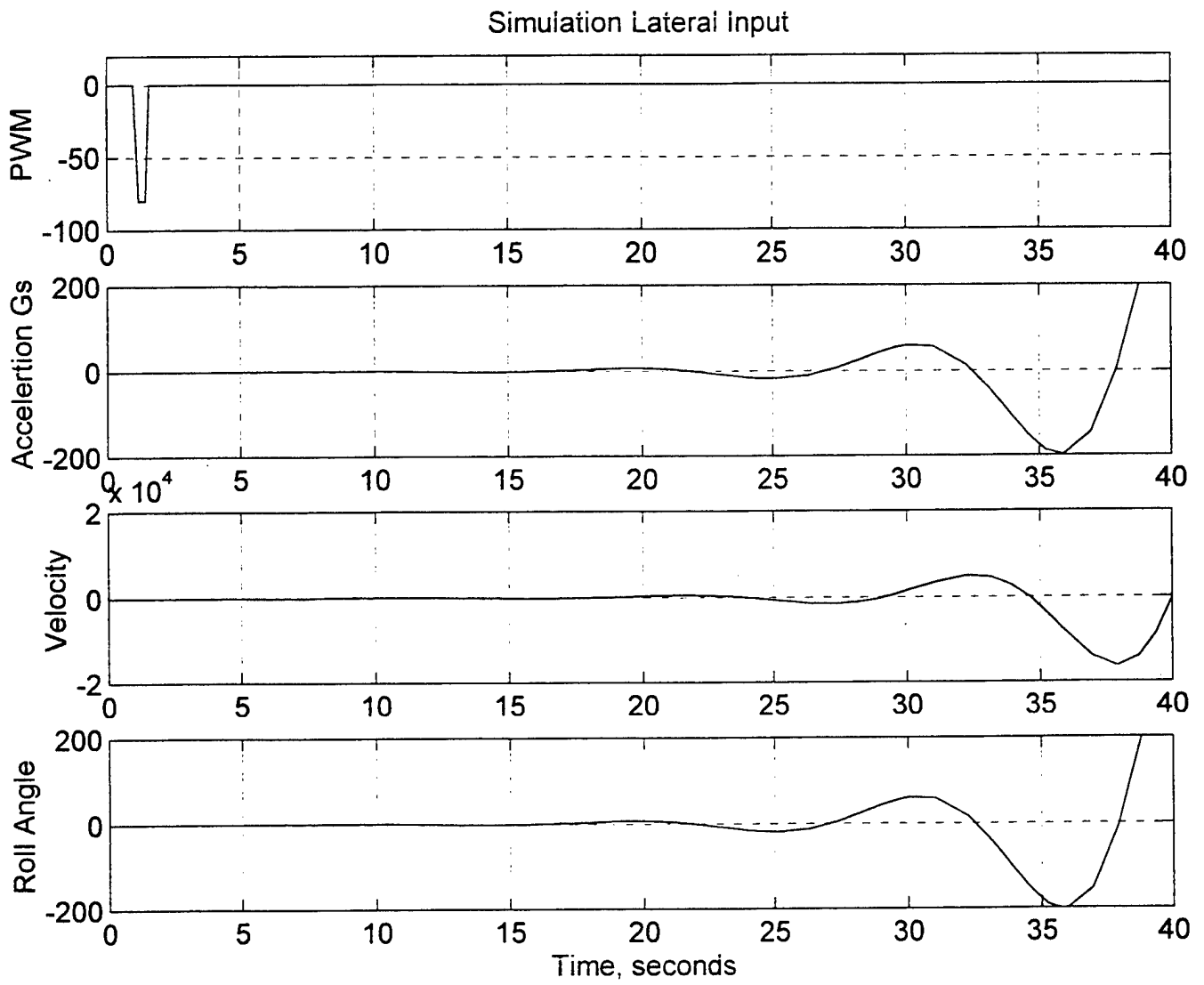


Figure 4.8 Long-Term Lateral Impulse Simulation

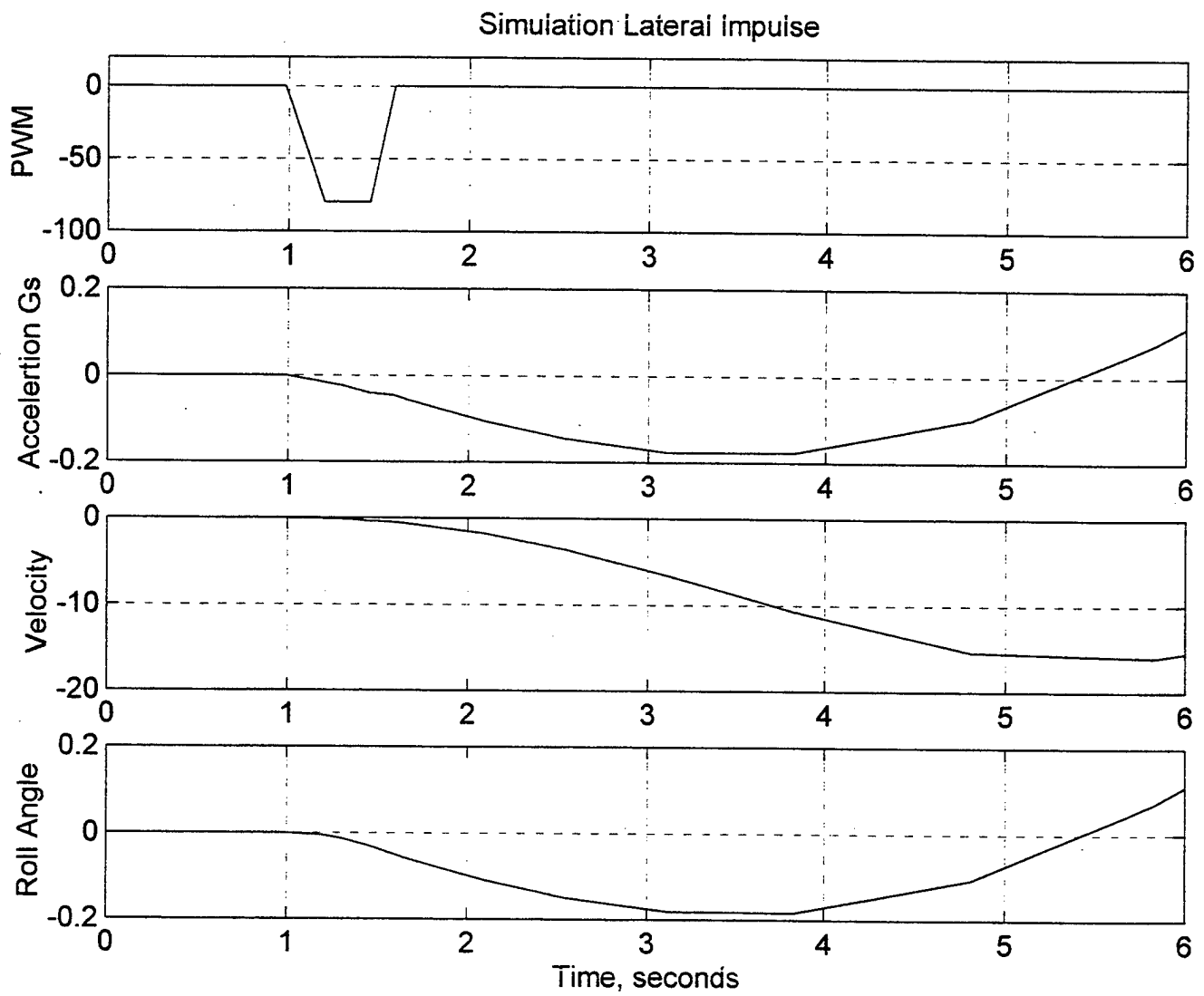


Figure 4.9 Short-Term Lateral Impulse Simulation

V. FLIGHT TESTING

A. INSTRUMENTATION OF FLIGHT VEHICLE

To obtain useful flight data to validate our simulation model, the UAV requires the incorporation of onboard instrumentation. Ideally, access to UAV airspeed, altitude, attitude, and acceleration would be available to accurately reconstruct air vehicle responses experienced during the test flight. For the initial flight-testing phase of the research, the goal was to obtain acceleration data in an out-of-ground effect (OGE) hover. The original instrumented configuration had an inertial measuring unit (IMU) with associated downlink telemetry devices mounted under the UAV on a modified landing gear with avionics rack. Reference 13 provides a detailed description of the avionics suite design.

The IMU, also referred to as an attitude, heading reference system (AHRS), provides bank (roll angle), elevation (pitch angle), heading (yaw angle), translational accelerations, and rotational accelerations along the X , Y and Z orthogonal axes. Due to space constraints, it is usually impossible to place the IMU at the ideal location, the air vehicle CG; therefore, the output data from the IMU must be transformed from its position to the aircraft's CG to the inertial reference system. Other onboard sensors can also be incorporated into the avionics suite to improve the collection of UAV response data, such as airspeed indicators and global positioning system (GPS) sensors.

B. PHYSICAL PARAMETER MODIFICATION

With the addition of instrumentation to the UAV, the performance and dynamic responses of the air vehicle will be changed due to the increased weight (mass) and altered mass distribution. Added weight will not only shift the CG position, but will change the mass-moments of inertia. Since the simulation model was developed about a 'trim condition', we must repeat the stability analysis to reflect the changes to the system's dynamic characteristics. In order to recalculate the new trim position, we must start by

changing the input parameters of the JANRAD program to obtain a new set of system and control matrices (F and G). In the following sections, we explain some of the methods used in determining the ‘new’ input variables.

1. Center of Gravity

The addition of onboard sensors and telemetry gathering equipment will alter the weight and mass distribution of the air vehicle. It is therefore necessary to make accommodations to our *simulation model* to reflect these changes experienced by the UAV. In addition to changing the vehicle weight, we must account for the altered mass distribution. The position of each additional component was determined with respect to the original UAV fuselage station (FS), waterline (WL) and butline (BL). The component mass was determined by using a calibrated scale and dividing by the gravity constant. An Excel[®] spreadsheet was developed to automatically account for the change in weight and CG position (Appendix F). The spreadsheet can easily be updated by simply annotating the addition of the added component on the worksheet; the component mass and location data are already determined. A second work sheet, discussed below, computes the change in UAV mass moment of inertia as a result of the new mass distribution.

2. Moments of Inertia

The change in mass distribution will alter the dynamic response of the UAV when perturbed from the trim position. A good example of the change in the moment of inertia is the spinning ice skater; with the hands extended, the skater spins slow, but when the hands (mass) are brought in close to the body (axis of rotation) the moment of inertia is reduced, and the rate of spin increases. Therefore, to accurately predict the dynamic response of the UAV to a control input, the moments of inertia will need to be recomputed accounting for the added mass and mass distribution. Using the Parallel Axis Theorem, the Excel program described above will automatically compute a new moment of inertia about the updated center of gravity (page 2 of Appendix F). For simplification, each added mass was treated as a point mass, i.e. the moment of inertia about its own CG

was neglected. The standard position of each component was located on the avionics rack with respect to the rack forward centerline.

After the moment of each component was determined, the new moment about the desired axis was obtained by using the relationship that the total moment of inertia of a body is equal to the sum of the individual parts about a common reference, i.e. the updated center of gravity (CG).

3. JANRAD Input Modifications

To obtain an updated set of 'plant' and control matrices from the JANRAD program, the process described in Chapter 3 will be repeated using the data obtained for the new UAV configuration. In addition to changing the CG position and mass-moments, additional parameters will need to be updated prior to running the analysis. Table 5.1 below provides a listing of all JANRAD input variables to be modified. The values used in the analysis are listed in Appendix B.

<i>Parameter</i>	<i>Units</i>	<i>JANRAD Input Screen</i>
Forward Velocity	[knots]	JANRAD "Edit Menu"
Temperature	[°F]	JANRAD "Edit Menu"
Pressure Altitude	[ft] MSL	JANRAD "Edit Menu"
Equivalent Flatplate Area	[ft ²]	JANRAD "Edit Menu"
Vertical Projected Area	[ft ²]	JANRAD "Edit Menu"
Gross Weight	Pounds [lbs.]	JANRAD "Edit Menu"
CG Position	[ft]	Stability & Cntl (3 of 3)
Mass-moments of Inertia	[slug-ft ²]	Stability & Cntl (3 of 3)
Main Rotor Rotational Velocity, Ω_{MR}	[rad/second]	JANRAD "Edit Menu"
Tail Rotor Rotational Velocity, Ω_{TR}	[rad/second]	Stability & Cntl (1 of 3)

Table 5.1 Altered Input Variables to JANRAD Program

C. REQUIRED MODIFICATIONS TO OUTPUT DATA

The output telemetry collected during the flight-testing does not accurately describe the responses of the body unless the information is taken with respect to the body (UAV) CG. Therefore, we must convert this data to the CG position of the body, then to the inertial reference, for comparison with the simulation model. Additionally, dependent upon the noise attenuation capabilities of the acceleration equipment used for collecting data, a considerable amount of vibration noise can be present in the output data, masking the desired translational accelerations.

1. Data Translations

Using a fully instrumented air vehicle, we desire access to all the states of the system (i.e. velocities, rotational rates and attitude). To accurately reconstruct the responses of the helicopter, it is necessary to translate these responses from the position of the IMU to the CG of the body. The IMU is the desired type of measurement device for collecting this data because of the depth of output information available. Due to vibration problems experienced during the initial instrumented flights, the avionics rack with associated measurement devices was unserviceable for mounting on the UAV during the later test flights. As an alternate method of collecting acceleration data, a Crossbow[®] three-axis accelerometer was temporarily mounted on the UAV to meet research completion requirements. It was necessary to tether, or hardwire, the UAV to the data collection ground station in order to collect the data from the sonar altimeter and accelerometer. With the vehicle tethered, the motion of the UAV was restricted to the limits of the umbilical. As mentioned above, we normally would use a transition matrix to transfer the data from the sensor to the CG of the air vehicle, but for this configuration, we must assume the accelerometer at the body CG. The translation of accelerometer data is not possible because the three-axis accelerometer does not provide angular rate information.

2. Vibration Noise Elimination

Unfortunately, the accelerometers utilized could not discriminate the desired translational accelerations from the high-frequency vibrations inherent of all helicopters. The major contributors of these additional vibrations are the main and tail rotors, and the helicopter power plant. The main rotor system acts like a “filter”, and only those vibrations with a frequency multiple of its rotational velocity (2P, 4P or 6P for a two bladed rotor) are translated through the system. Figure 5.1 (top figure) shows a sample of some raw acceleration data. It is difficult to identify the translational accelerations in response to pilot control inputs. Therefore, to make the acceleration data useful, it was necessary to filter out these extraneous, high frequency accelerations. Initially, a spectral density analysis was used to confirm the main rotor rotational frequency of 27 Hertz. With this information, the raw data could be filtered to eliminate the higher frequency noise from the desired acceleration data. Accelerometer data was filtered using a 4th order Butterworth Low-pass filter with a cut-off frequency of 12 rad/sec. The filtered data (Figure 5.1 bottom plot) can now be used to identify the aircraft responses for analysis.

D. FLIGHT DATA ANALYSIS

The goal during the flight-testing phase was to replicate system responses available from the simulation model. The Simulink model described in Chapter 3 allows the system to be perturbed about a trim position by either a control *step* input, *impulse* or *doublet* (control input reversal). It was desired to have the UAV pilot replicate the identical type of inputs as were used in the simulations. This would simplify the comparison of UAV responses to those of the simulation model. Because of the limitations imposed by the “umbilical” used to transfer acceleration and altitude data to the ground station, the inputs to the UAV had to be minimized to maintain an acceptable margin of safety for the UAV. The test runs conducted included a series of longitudinal and lateral cyclic and collective doublets. Figure 5.2 (upper plot) shows the type of input used in the simulation trials. The

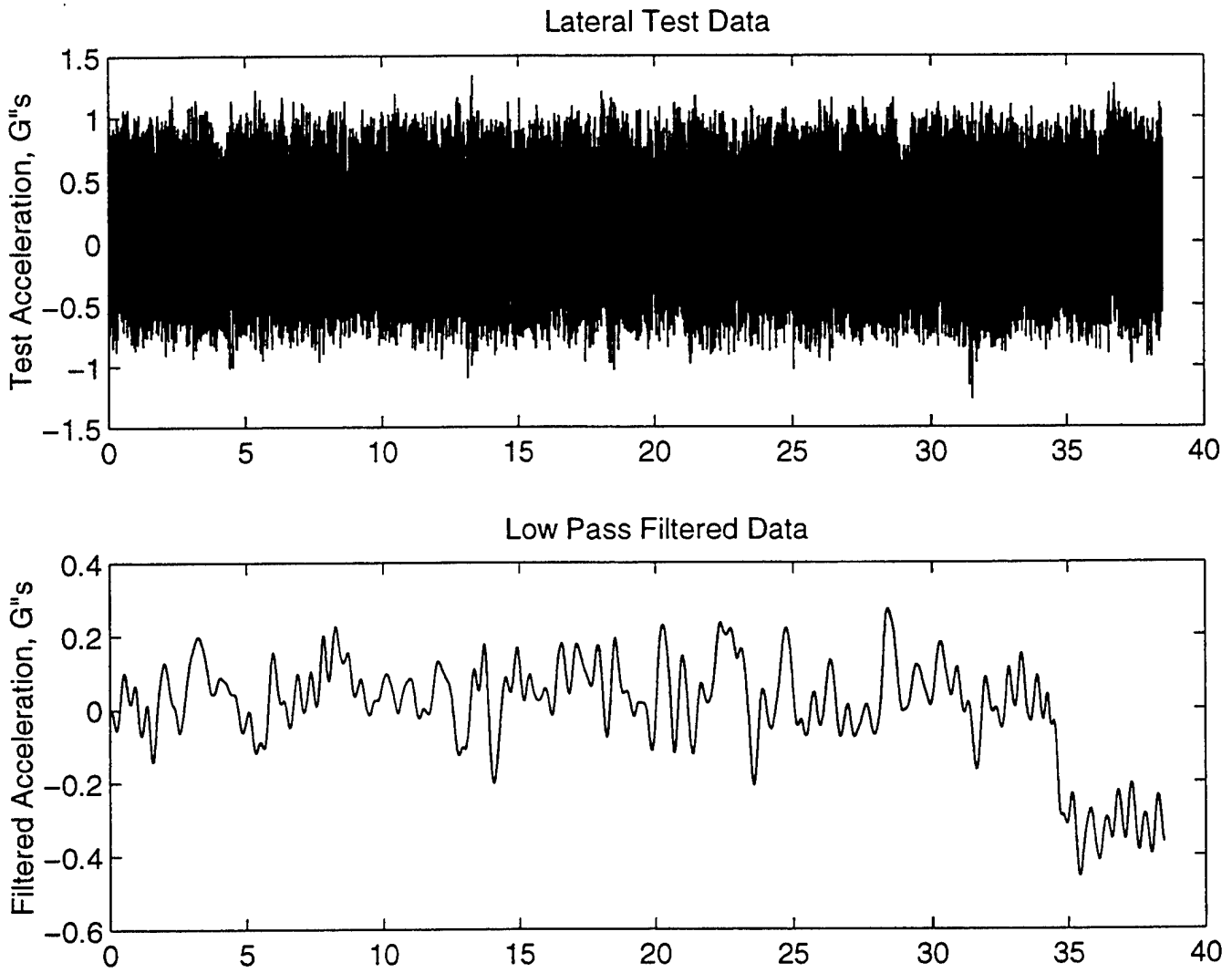


Figure 5.1 Comparison of Raw Acceleration Data with Filtered Data

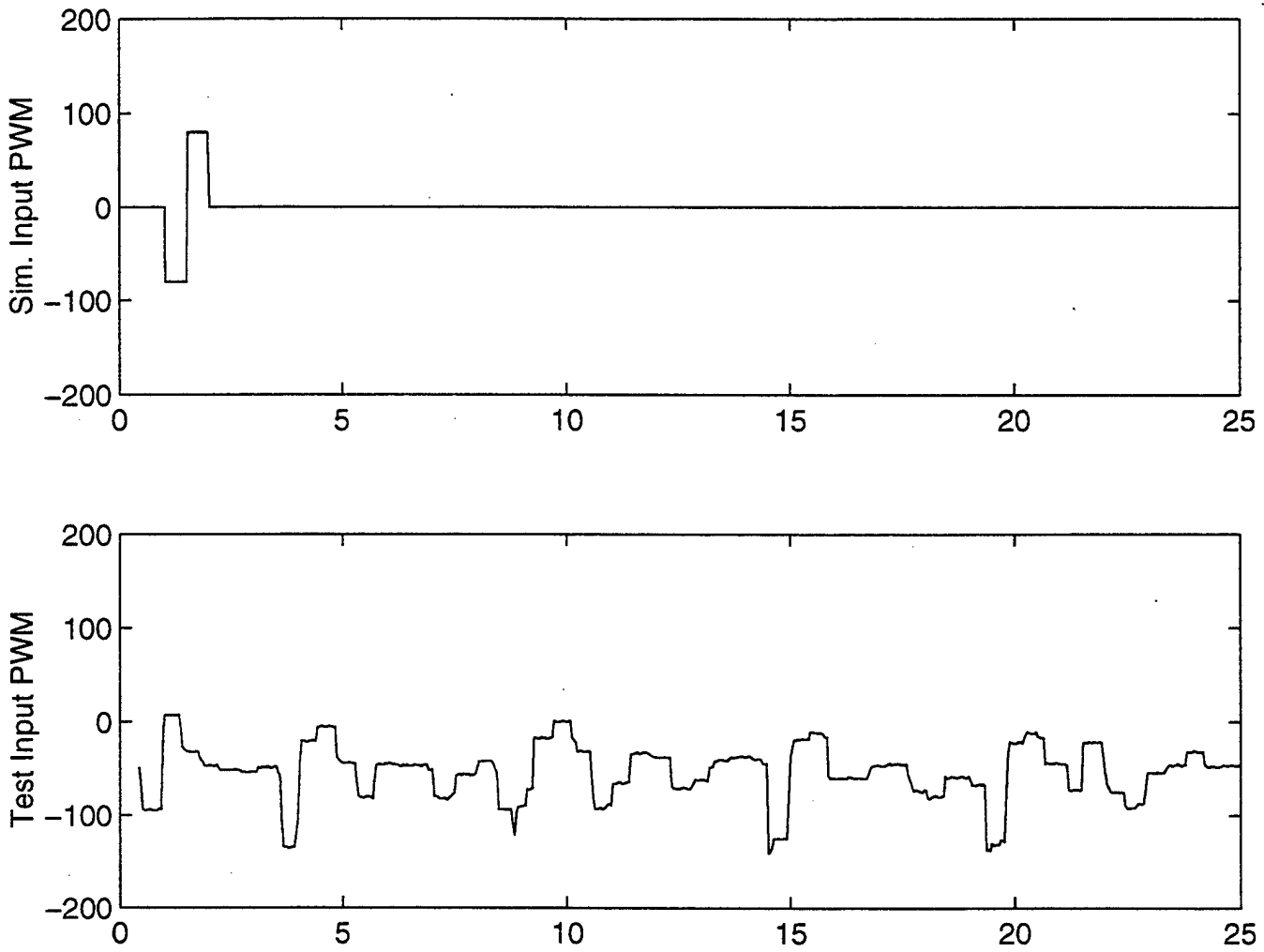


Figure 5.2 Comparison of Simulation Input to Test-Flight Input

lower plot shows the actual PWM (corrected about a trim position) from an actual test flight. It is apparent that comparing the responses of the model with the UAV using these different types of inputs would not be realistic. Therefore, in the comparison of the simulation model with the actual air vehicle required subjecting the *simulation model* to the same input as the UAV was subjected. The test flight PWM collected by the ground station was converted to a MATLAB compatible format, then input into the Simulink model for each simulation run.

E. COMPARISON OF SIMULATION AND FLIGHT DATA

The purpose of the flight-testing was the verification of the simulation model, and the validation of the Sonar Altimeter operation as the subject of Reference 13; therefore, the limited test time was divided between meeting both objectives providing limited test flight-data. Two test runs involved subjecting the UAV to collective doublets, while the lateral and longitudinal doublets were only examined on one trial each. Control input data and UAV accelerations were collected on separate data loggers which were not synchronized and used different sampling rates; therefore, the data had to be synchronized by hand to yield an accurate comparison between simulation and test data. Many of the figures below are plotted versus sampling rate, or filtering rate vice *time* in seconds. All accelerations are given in “G’s” with altitude given in feet above ground level.

The first mode we will analyze is the two vertical collective doublet test-flights. Figure 5.3 shows the actual collective PWM input from the test-flight and simulation, the simulation responses in G’s, the filtered acceleration data in the vertical axis and the altimeter data from the sonar altimeter. Figure 5.4 displays the same type of data for the second collective doublet flight. For both flights, it is apparent the simulation model tracks closely the actual responses of the UAV. Note: an *increase* in collective leading to a positive “G” and climb is indicated by a *decrease* in the PWM signal.

The next series of flight-test data is for the lateral cyclic doublet. Figure 5.5 shows the lateral input, the simulation acceleration and the lateral test G’s loads. The simulation

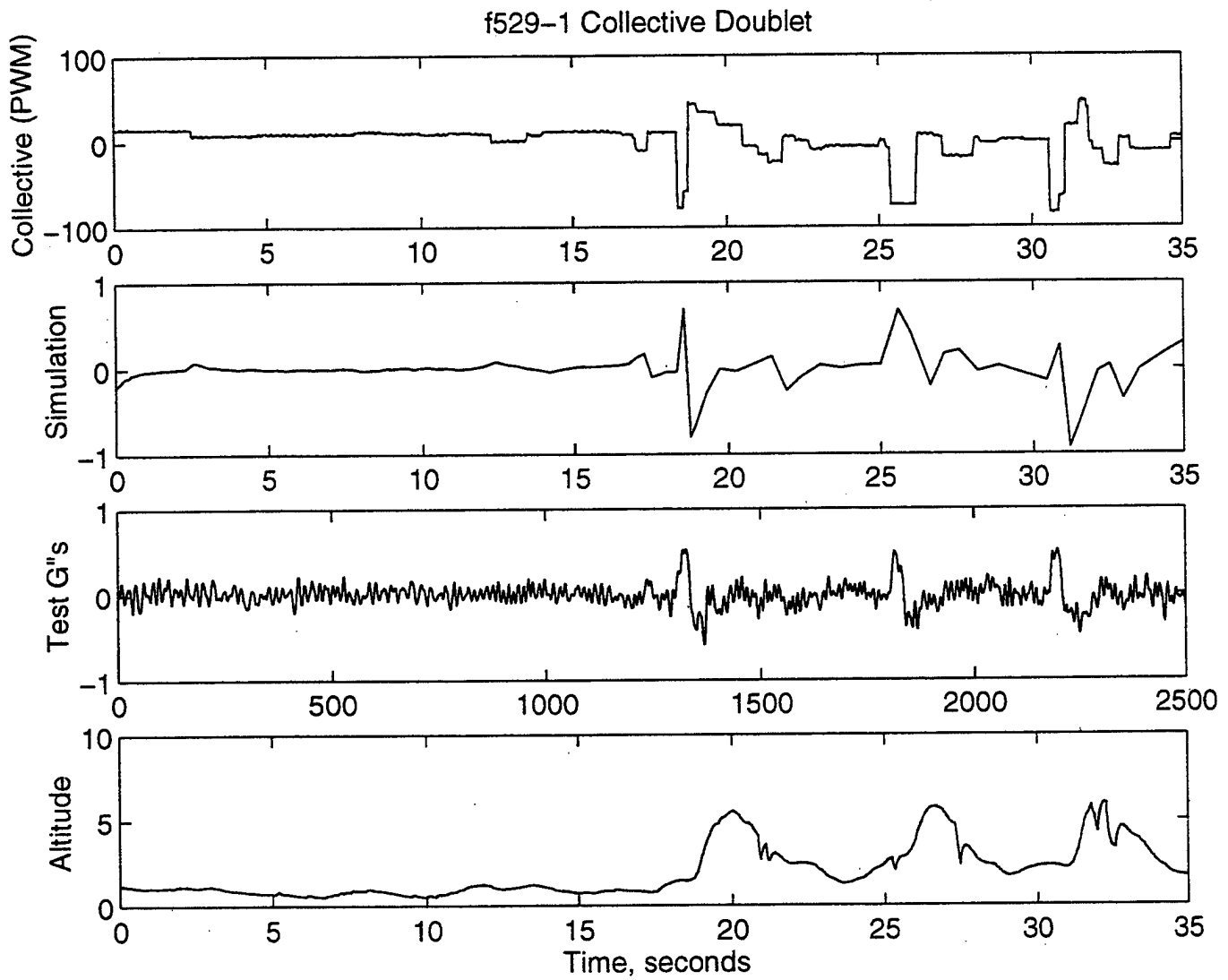


Figure 5.3 Vertical Response to a Collective Doublet (Flight 1)

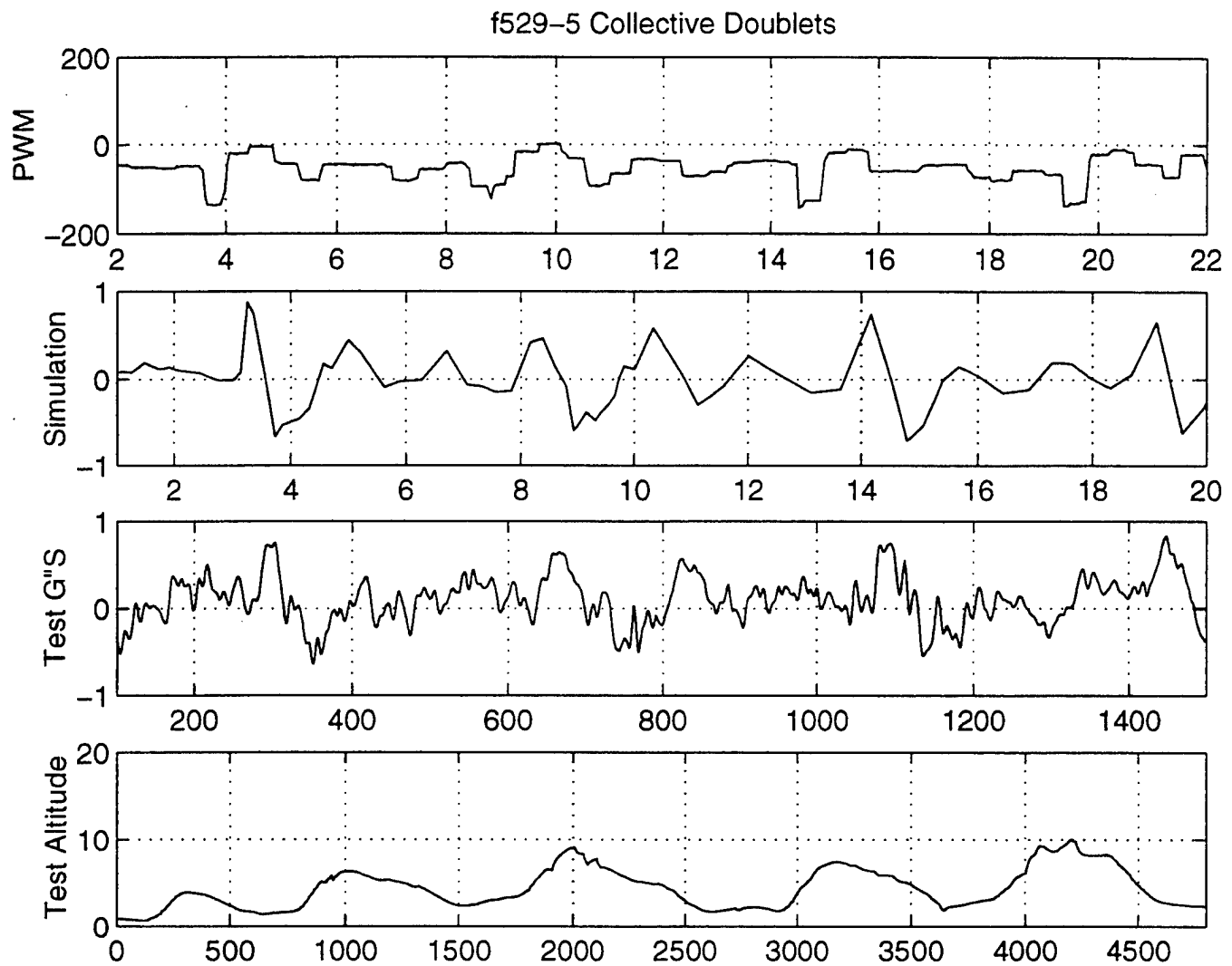


Figure 5.4 Vertical Response to a Collective Doublet (Flight 5)

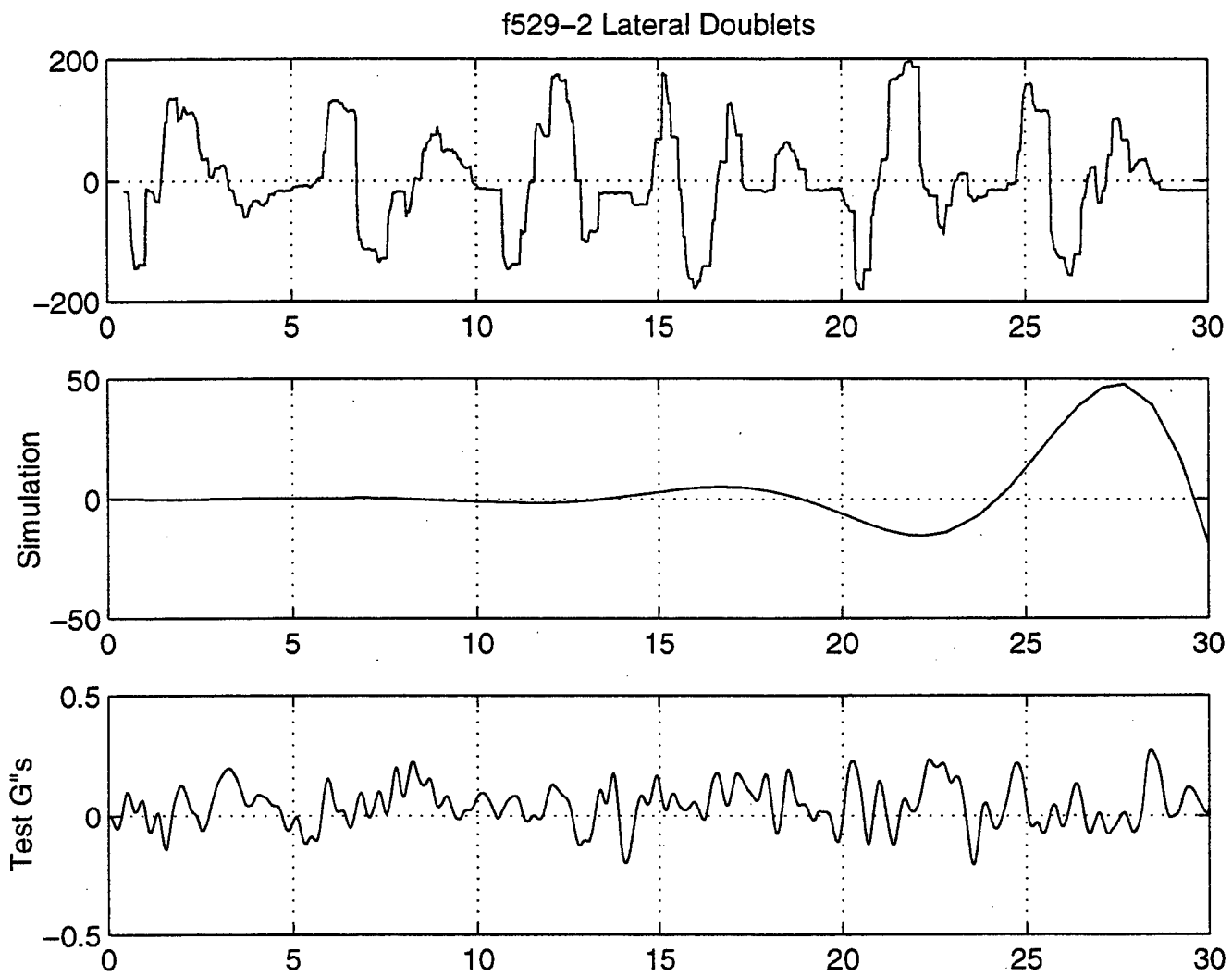


Figure 5.5 Lateral Response to a Lateral Cyclic Doublet (Long-Term)

model, because it is unstable in the lateral mode, yields divergent oscillations as time progresses. Therefore, the large scale used on the y-axis gives no indication of the initial lateral accelerations of the model. The period of the oscillations should be noted since it is on the order of 10 seconds, equal to the period of the unstable dutch-roll mode. To determine the initial response of the model due to the cyclic control input, we have replotted the same test data on a shortened time scale (Figure 5.6). From the figure, we can determine that the initial response of the simulation model is of the same acceleration magnitude as the test UAV.

Subjecting the simulation model to a longitudinal cyclic doublet, the results were similar with those referred to above for the lateral mode. Figure 5.7 shows the long-term acceleration ($G'S$) and pitch angle (radians) response of the simulation model and UAV to a series of longitudinal doublets. Again we note the simulation model starts divergent oscillations due to the first longitudinal doublets leading to undetectable initial response data. Of note is the period of the acceleration and pitch angle oscillations; from Chapter 4, we identified the phugoid mode to have a period of approximately 14 seconds which is shown in the figure. The same flight data was plotted for a short duration (Figure 5.8) yielding initial responses of the simulation model similar to the initial responses of the UAV.

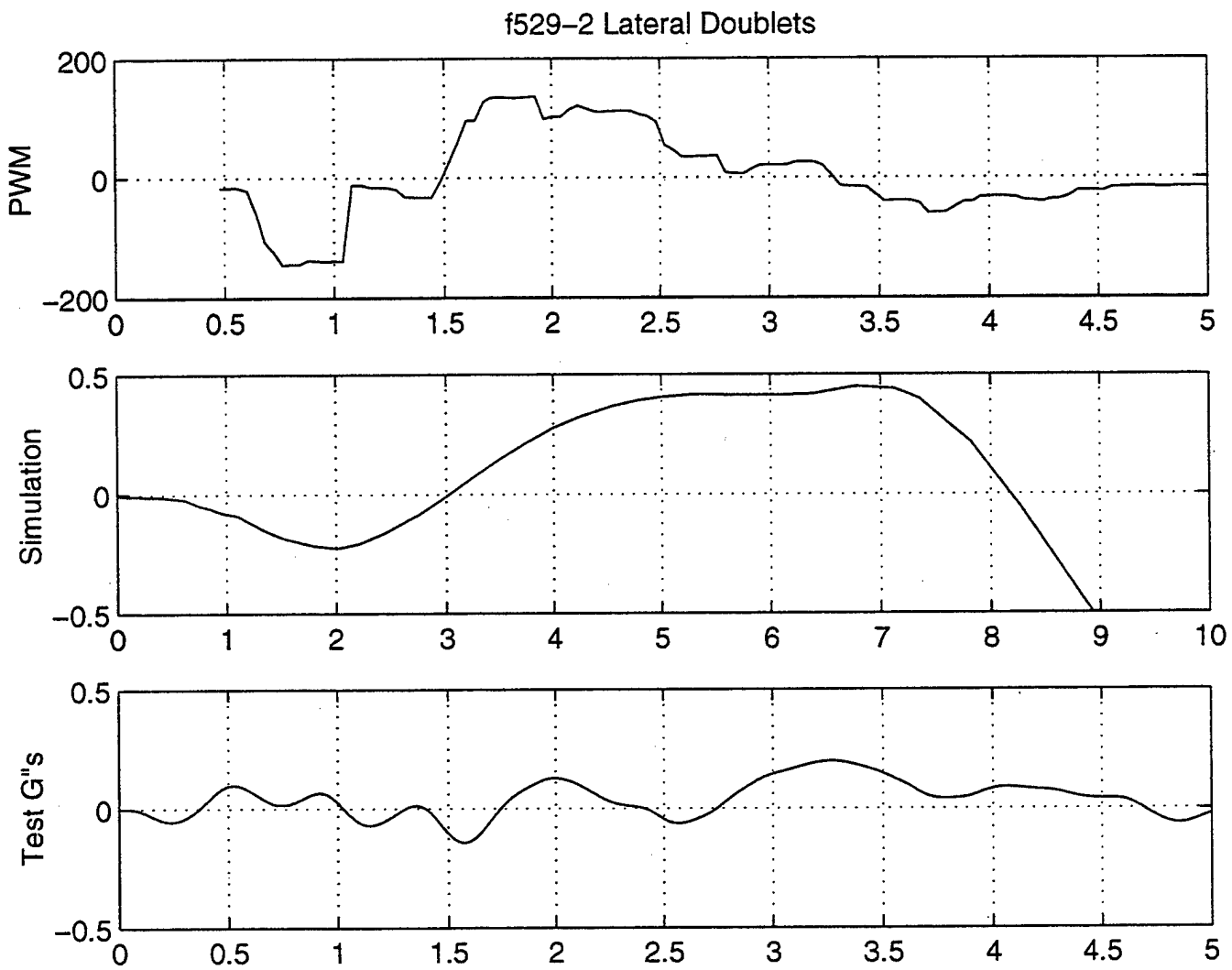


Figure 5.6 Lateral Response to a Lateral Cyclic Input (Short-Term)

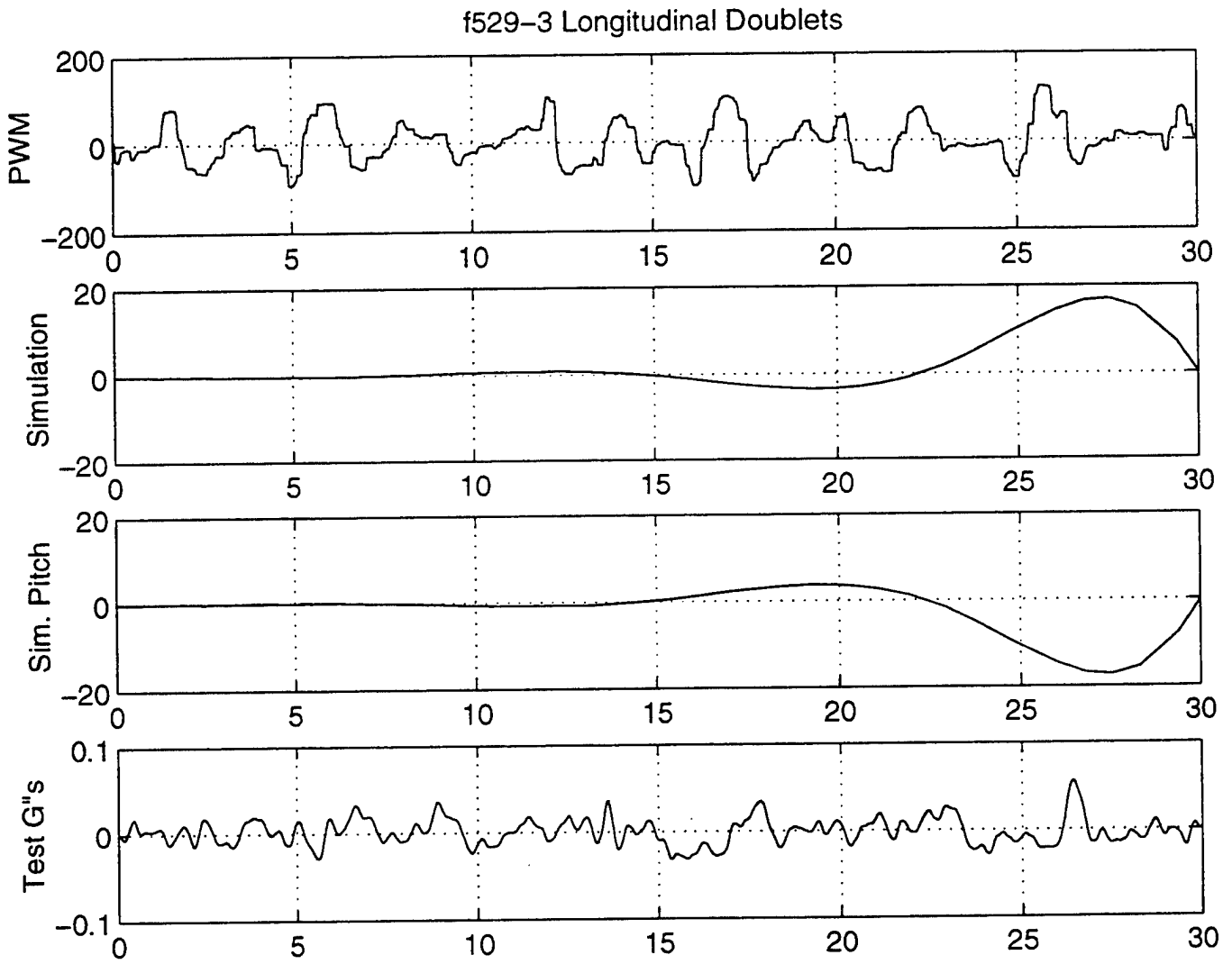


Figure 5.7 Longitudinal Response to a Longitudinal Cyclic Input (Long-Term)

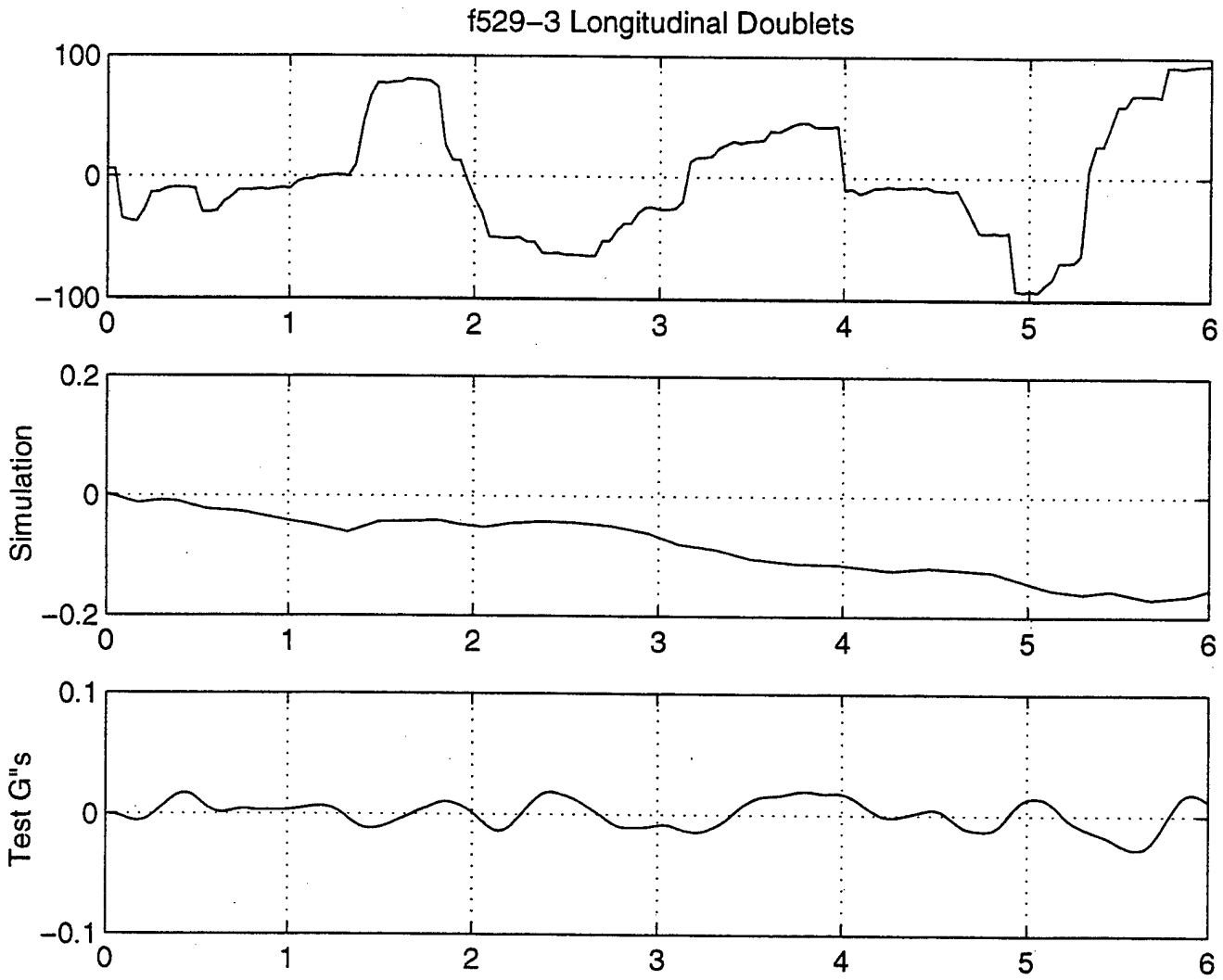


Figure 5.8 Longitudinal Response to a Longitudinal Cyclic Input (Short-Term)

VI. CONCLUSIONS AND RECOMMENDATIONS

A. CONCLUSIONS

The rotary wing flight vehicle presents an interesting and complicated dynamic system for the stability and control analyst. To accurately model this complicated, non-linear, nine-degree of freedom (DoF) system requires complex algorithms and analysis. A common approximation of using a linear, 6 DoF system is useful for preliminary analysis using small perturbations about a trim condition. It was the effort of this research to use a linear analysis to develop a simulation model of the Bergen rotary wing UAV capable of predicting its responses to pilot controlled inputs.

The linear model developed was capable of simulating the vertical accelerations experienced by the UAV along the vertical axis when subjected to the identical collective inputs from the flight-tests. Problems arose when the model was subjected to inputs along the lateral and longitudinal axes. The initial response of the model along these axes followed the UAV for response direction and magnitude of accelerations. But, over the long term, inherent instabilities of the UAV and simulation model led to divergent behavior when perturbed from the trim condition. The time period of these unstable oscillations was within the capabilities of the UAV pilot to control, but complicated matters for the simulation model. As these unstable perturbations persisted, additional inputs were made to maintain control of the UAV which further perturbed the model which was, at this point, no longer in a trim condition.

The linear model could be used in the development of an altitude controller should the vehicle be used in a hover or in slow near-hovering flight. A more robust, non-linear model is needed to accurately predict the dynamic response of the UAV in other flight regimes.

B. RECOMMENDATIONS

Because of the complexity of the rotary wing vehicle with its interacting components and cross-coupled dynamic responses, a non-linear model is presumably needed to accurately predict the UAV responses to controller inputs. To accomplish this, the UAV would require proper instrumentation providing access to all states of the system. With the collection of flight data, one of the many system identification programs could be used to identify the system, and modify the current model or develop a completely new one.

To ease the complexity of the model responses, only a single test-flight control signal was input at any time. With a more robust model, it may be possible to apply all four inputs to the model from the control data collected during the test-flights. Additionally, an attempt was made to more closely model the actual UAV by the incorporation of a feedback stabilization yaw-damper. To facilitate remote-pilot operation of the UAV, a yaw rate gyro with feedback control is incorporated on the Bergen RC helicopter. This eliminated aircraft yaw during large power changes. With the feedback controller on the simulation model, the initial yaw angle experienced was reduced, but the inherent instabilities of the system were not eliminated. Applying feedback controllers to the unstable axes may increase the desired response of the simulation model.

Although, all these capabilities currently exist, and are used to control a wide range of UAV platforms, this research, though not groundbreaking, provides the student a foundation for the development of simulation models and the control of flight vehicles. It is imperative to expand on the work presented in this report, and that presented in Reference 13 to fully realize the potential of past, present and future NPS endeavors in this area.

APPENDIX A: STABILITY AND CONTROL DERIVATIVES

$$\mathbf{A} = \begin{bmatrix}
 X_u & X_w - Q_e & X_q - W_e & X_v + R_e & X_p & X_r + V_e \\
 Z_u + Q_e & Z_w & Z_q + U_e & Z_v - P_e & Z_p - V_e & Z_r \\
 M_u & M_w & M_q & M_v & M_p - 2P_e I_{xz} / I_{yy} & M_r + 2R_e I_{xz} / I_{yy} \\
 0 & 0 & \cos \Phi_e & 0 & 0 & -\sin \Phi_e \\
 Y_u - R_e & Y_w + P_e & Y_q & Y_v & Y_p + W_e & Y_r - U_e \\
 L'_u & L'_w & L'_q + k_1 P_e - k_2 R_e & L'_v & L'_p + k_1 Q_e & L'_r - k_2 Q_e \\
 0 & 0 & \sin \Phi_e \tan \Theta_e & \Omega_a \sec \Theta_e & 1 & \cos \Phi_e \tan \Theta_e \\
 N'_u & N'_w & N'_q - k_1 R_e - k_3 P_e & N'_v & N'_p - k_3 Q_e & N'_r - k_1 Q_e
 \end{bmatrix}$$

$$\mathbf{B} = \begin{bmatrix}
 X_{\Theta_0} & Z_{\Theta_0} & M_{\Theta_0} & 0 & Y_{\Theta_0} & L'_{\Theta_0} & 0 & N'_{\Theta_0} \\
 X_{\Theta_{1s}} & Z_{\Theta_{1s}} & M_{\Theta_{1s}} & 0 & Y_{\Theta_{1s}} & L'_{\Theta_{1s}} & 0 & N'_{\Theta_{1s}} \\
 X_{\Theta_{1c}} & Z_{\Theta_{1c}} & M_{\Theta_{1c}} & 0 & Y_{\Theta_{1c}} & L'_{\Theta_{1c}} & 0 & N'_{\Theta_{1c}} \\
 X_{\Theta_{0r}} & Z_{\Theta_{0r}} & M_{\Theta_{0r}} & 0 & Y_{\Theta_{0r}} & L'_{\Theta_{0r}} & 0 & N'_{\Theta_{0r}}
 \end{bmatrix}$$

Appendix A: Stability and Control Derivatives (A and B Matrices)

Here is a complete listing of the stability and control derivatives that comprise the stability and control matrices (A and B, respectively) [Ref. 1].

APPENDIX B. JANRAD INPUT DATA

The following is a comprehensive listing of all input variables used in the JANRAD Performance and JANRAD Stability analysis programs.

*** JANRAD Performance Input Data ***

Forward velocity = 0 kts	Vertical projected area = 1.71 ft ²
Temperature = 60 degs F	Wing area = 0.00 ft ²
Pressure altitude = 100 ft	Wing span = 0.00 ft
Gross weight = 19.16 lbs	Wing CL = 0.00
Number of blades = 2	Wing CDo = 0.0000
Rotor radius = 2.83 ft	Wing efficiency factor = 0.00
Blade mean chord = 0.20 ft	Horizontal tail area = 0.12 ft ²
Blade twist = 0.00 degs	Horizontal tail span = 0.66 ft
Blade airfoil = VR-12	Horizontal tail CL = 0.00
Blade lift curve slope = 5.73	Horizontal tail CDo = 0.0050
Blade weight = 0.42 lbs	Vertical tail area = 0.22 ft ²
Rotational velocity = 164.00 rads/sec	Vertical tail span = 0.92 ft
Blade grip length = 0.27 ft	Vertical tail CL = 0.00
Hinge offset = 0.00 ft	Vertical tail CDo = 0.0050
Equivalent flat plate area = 0.67 ft ²	Auxiliary thrust = 0 lbs

*** JANRAD Stability Input Data ***

*** INPUT DATA (screen 1 of 8) ***

Flight Conditions

Forward velocity = 0 kts
Temperature = 60 degs F
Pressure altitude = 100 ft
Auxiliary thrust = 0 lbs

Fuselage

Gross weight = 19.16 lbs
Ixz = 0.000 slug ft²
Downwash ratio = 1.50

Equivalent flat plate area = 0.67 ft²
Vertical projected area = 1.35 ft²
CG height above waterline = -0.23 ft
CG fuselage station = 1.06 ft
CG position right of butline = 0.00 ft
Ixx = 0.719 slug ft²
Iyy = 1.433 slug ft²
Izz = 2.594 slug ft²

** INPUT DATA CONTINUED (screen 2 of 8) **

Main Rotor

Number of blades = 2

Rotor radius = 2.83 ft

Blade twist = 0.00 degs

Blade airfoil = VR-12

Blade lift curve slope = 5.73

Blade weight = 0.42 lbs

Rotational velocity = 164.00 rads/sec

Blade grip length = 0.27 ft

Hinge offset = 0.00 ft

Flapping moment of inertia = 0.034 slug ft²

Hub height above waterline = 0.75 ft

Hub fuselage station = 1.25 ft

Hub position rt of butline = 0.00 ft

Mast incidence = 0.00 deg

*** INPUT DATA CONTINUED (screen 3 of 8) ***

Tail rotor (zeros if using NOTAR)

Number of blades = 2.0

Blade chord = 0.01 ft

Blade radius = 0.52 ft

Lift curve slope = 5.73

Rotational velocity = 754.00 rad/sec

Hub fuselage station = 4.730 ft

Hub position rt of butline = -0.188 ft

Delta-3 angle = 0.00 deg

Blade twist = 0.00 deg

Hub height above waterline = 0.156 ft

Flapping moment of inertia = 0. slug ft²

*** INPUT DATA CONTINUED (screen 4 of 8) ***

NOTAR (zeros if using tail rotor)

Height above waterline = 0.0 ft²

Fuselage station = 0.0 ft²

Position right of butline = 0.0 ft²

NOTAR boom diameter = 0.0 ft²

Swirl angle at boom = 0.00 deg

Maximum thruster force = 0.0 lbs

Thrust fuselage station = 0.0 ft²

*** INPUT DATA CONTINUED (screen 5 of 8) ***

Wing

Area = 0.0 ft²

Span = 0.0 ft

CL = 0.00

CDo = 0.0000

Tip cord = 0.0 ft

Root cord = 0.0 ft

Rotor downwash ratio = 0.00

Fuselage downwash ratio = 0.00

Wing efficiency factor = 0.00

Zero lift angle = 0.00 deg

Angle of incidence = 0.00 deg

Lift curve slope = 0.00

Height above waterline = 0.0 ft

Fuselage station = 0.0 ft

Position right of butline = 0.0 ft

*** INPUT DATA CONTINUED (screen 6 of 8) ***

Horizontal tail

Area = 0.12 ft²

Span = 0.66 ft

CL = 0.00

CDo = 0.0050

Zero lift angle = 0.00 deg

Angle of incidence = 0.00 deg

Lift curve slope = 3.4

Height above waterline = 0.20 ft

Fuselage station = 3.70 ft

Position right of butline = 0.00 ft

Dynamic pressure ratio = 0.60

Rotor downwash ratio = 1.50

Fuselage downwash ratio = 0.06

*** INPUT DATA CONTINUED (screen 7 of 8) ***

Vertical tail

Area = 0.22 ft²

Span = 0.92 ft

CL = 0.00

CDo = 0.0050

Height above waterline = 0.04 ft

Fuselage station = 4.52 ft

Position right of butline = 0.05 ft

Zero lift angle = 0.00 deg

Maximum Cl = 0.8

Dynamic pressure ratio = 0.60

Lift curve slope = 3.44

*** INPUT DATA CONTINUED (screen 8 of 8) ***

Rigging

Long cyclic pitch/inch defl = 0.03 deg/in

Lat cyclic pitch/inch defl = 0.01 deg/in

Collective pitch/inch defl = -0.02 deg/in

Tail rotor pitch change/defl = -0.09 deg/unit

Max deflection of control from neutral for NOTAR = 0.00 units

Displacement of anti-torque control until full rudder = 0.00 units

APPENDIX C. MASS-MOMENTS OF INERTIA CALCULATIONS

This is a listing of the variables used to determine the mass-moments of inertia for the Bergen UAV using the technique outlined in Reference 7.

For Trials #1, 2 and 3, the following relation was used:

$$I_{CG} = \frac{[W_M + W_S]z_{M+S}}{4\pi^2} p^2_{M+S} - \frac{W_M z_M^2}{g} - \frac{W_S z_S^2}{g}$$

<i>Component</i>	<i>Variable</i>	<i>Trial 1</i>		<i>Trial 2</i>		<i>Trial 3</i>
		<i>I_{XX}, I_{YY}</i>	<i>I_{ZZ}</i>	<i>I_{XX}, I_{YY}</i>	<i>I_{ZZ}</i>	<i>I_{XX}, I_{YY}</i>
Model Weight	W_M	15.57	15.57	16.44	16.44	16.65
Support Weight	W_S	2.44	1.61	0	0	0
Distance to support CG	Z_S	6.584	6.584	0	0	0
Distance to model CG	Z_M	13.23	13.41	14.01	13.45	4.0
Distance to system CG	Z_{M+S}	12.33	12.77	14.01	13.45	4.0

* Test set-up on Trial 3 lacked sufficient clearance to check the I_{ZZ} mode.

where,

$$Z_{M+S} = \frac{W_S Z_S + W_M Z_M}{W_{M+S}}$$

The resulting system periods are listed below for each mode;

<i>Trial</i>	<i>I_{XX}</i>	<i>I_{YY}</i>	<i>I_{ZZ}</i>
1	4.0 sec	4.01 sec	4.0 sec
2	4.15 sec	4.13 sec	4.10 sec
3	2.24 sec	2.267 sec	----

APPENDIX D. BEAM DEFLECTION EXPERIMENTAL DATA

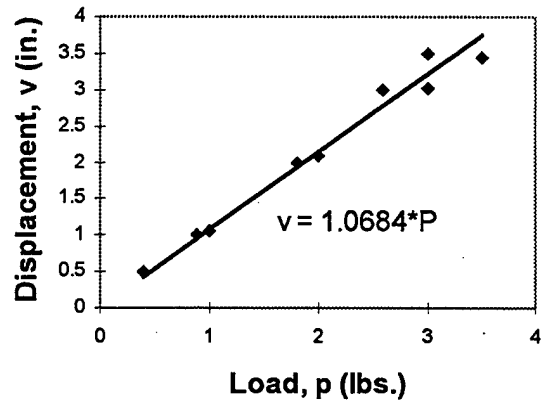
This appendix provides the experimental data and results obtained for the stiffness, EI , of the main rotor blade using the relation below.

load, lbs.	deflection, v	$EI (10^6)$
1	1.063	0.008906
2	2.094	0.009042
3	3.03	0.009373
3.5	3.44	0.009632
0.4	0.5	0.007573
0.9	1	0.00852
1.8	2	0.00852
2.6	3	0.008204
3	3.5	0.008114

$$EI_{\text{Avg.}} = 0.008654 \quad (*10^6)$$

$$EI = \frac{PL^3}{3v}$$

Beam Deflection vs. Load



APPENDIX E. STATE-SPACE MATRICES

The following is a listing of the output state-space matrices calculated using the JANRAD Stability program.

$$A = \begin{bmatrix} -0.0091 & 0 & 0.4862 & -32.2000 & -0.0020 & -0.1538 & 0 & 0 \\ 0 & -1.8778 & 0 & 0.0002 & 0 & 0 & 1.5383 & 0 \\ 0.0037 & -0.1477 & -0.1972 & 0 & 0.0005 & 0.0624 & 0 & .0012 \\ 0 & 0 & 0.9989 & 0 & 0 & 0 & 0 & .0478 \\ 0.0020 & 0 & -0.1538 & 0.0000 & -0.0180 & -0.4896 & 32.1632 & .0327 \\ 0.0016 & 0 & -0.1243 & 0 & -0.0101 & -0.3941 & 0 & .0104 \\ 0 & 0 & 0.0000 & 0 & 0 & 1.0000 & 0 & 0 \\ 0 & -0.1270 & 0 & 0 & 0.0075 & 0.0029 & 0 & -5.2074 \end{bmatrix}$$

$$B = \begin{bmatrix} 0.0116 & 0.0000 & 0 & 0 \\ 0 & 0.3864 & 0 & 0 \\ -0.0047 & 0.0304 & 0 & -0.0040 \\ 0 & 0 & 0 & 0 \\ 0 & 0 & 0.0052 & -0.0037 \\ 0 & 0 & 0.0042 & -0.0012 \\ 0 & 0 & 0 & 0 \\ 0 & -0.0125 & 0 & 0.0031 \end{bmatrix}$$

APPENDIX F. CENTER OF GRAVITY AND MOMENT OF INERTIA

The following two EXCEL spreadsheets calculate the changes in CG position, as well as, Moments of Inertia with the addition of measurement devices. All inputs are made to Sheet 1.

Center of Gravity Spreadsheet

This spreadsheet will calculate displacement of the Center of Gravity with the addition of flight-test instrumentation. The new gross weight and center of gravity location can be changed in the JANRAD input file (pg.3 of 3).

Input a "1" into the 3rd column if the component is installed.
 **Input values of X, Y, & Z are in inches from front-centerline of avionics rack.

Component	Weights	0/1	Weight	X	Y	Z
UAV	16.44	1	16.44	14.25	0	12.19
Gear Mod	5.64	0	0	12.2	0	2.1
Original Gear	-0.62	0	0	11	0	6.5
Fuel	0.855	1	0.855	3.5	0	7
IMU	2	0	0	18	0	2.59
SONALT TX	0.19	0	0	10.5	-5	-0.5
SONALTCircuit	0.42	0	0	19	-7	3.5
Temp SONALT	1.2	1	1.2	3.5	0	5.5
Freewaves	0.75	0	0	12	4.5	0.33
Power Panel	1.66	0	0	18	6.5	3.5
Battery	2.32	0	0	18	-4	4
Camera	3	0	0	3	0	0
Autopilot	0.485	0	0	0	0	0
DGPS Antenna		0				
DGPS Receiver		0				
Misc.		0				
Basic Helo Moments [slug-ft²]				0.0709	0.3967	1.88

New C.G. Position*
 x'= 1.194
 y'= 0.000
 z'= 2.424
 *WRT reference point.

Gross Weight 18.495 lbs.

Moment of Inertia Spreadsheet

This spreadsheet will automatically calculate the new Moments of Inertia of the modified UAV based upon inputs on the preceding page.

Note: Do NOT change inputs to this sheet.

<i>Basic Helo</i>	I_{xx}	I_{yy}	I_{zz}	[slug-ft ²]	x' = 1.194
	0.0709	0.3967	1.88		y' = 0.000
Modified Helo	0.086	0.457	1.926	[slug-ft ²]	z' = 2.424

Component	Weight	mass	X	$m(y^2+z^2)$	Y	$m(x^2+z^2)$	Z	$m(x^2+y^2)$
<i>UAV</i>	16.44	0.511	-1.194	0.232	0.000	0.960	-0.674	0.728
<i>Gear Mod</i>	0	0.000	0.856	0.000	0.000	0.000	9.416	0.000
<i>Original Gear</i>	0	0.000	2.056	0.000	0.000	0.000	5.016	0.000
<i>Fuel</i>	0.855	0.027	9.556	0.542	0.000	2.966	4.516	2.424
<i>IMU</i>	0	0.000	-4.944	0.000	0.000	0.000	8.926	0.000
<i>SONALT TX</i>	0	0.000	2.556	0.000	-5.000	0.000	12.016	0.000
<i>SONALT Circuit</i>	0	0.000	-5.944	0.000	-7.000	0.000	8.016	0.000
<i>Temp SONALT</i>	1.2	0.037	9.556	1.349	0.000	4.752	6.016	3.403
<i>Freewaves</i>	0	0.000	1.056	0.000	4.500	0.000	11.186	0.000
<i>Power Panel</i>	0	0.000	-4.944	0.000	6.500	0.000	8.016	0.000
<i>Battery</i>	0	0.000	-4.944	0.000	-4.000	0.000	7.516	0.000
<i>Camera</i>	0	0.000	10.056	0.000	0.000	0.000	11.516	0.000
<i>Autopilot</i>	0	0.000	13.056	0.000	0.000	0.000	11.516	0.000
<i>DGPS Antenna</i>	0	0.000	13.056	0.000	0.000	0.000	11.516	0.000
<i>DGPS Receiver</i>	0	0.000	13.056	0.000	0.000	0.000	11.516	0.000
<i>Misc.</i>	0	0.000	13.056	0.000	0.000	0.000	11.516	0.000

				2.122		8.678		6.556
Gross Weight	18.495							

LIST OF REFERENCES

1. Padfield, Gareth D., *Helicopter Flight Dynamics: The Theory and Application of Flying Qualities and Simulation Modeling*, AIAA Educational Series, Washington DC, 1996.
2. Prouty, Raymond W., *Helicopter Performance, Stability and Control*, Krieger Publishing, Malabar, FL, 1995.
3. Hostetler, Ray, *Ray's Complete Helicopter Manual*, 2nd Ed., RC Modeler Corp., Sierra Madre, CA, 1990.
4. Nicholson, Robert K. Jr., *Computer Code for Interactive Rotorcraft Preliminary Design Using a Harmonic Balance Method for Rotor Trim*, Masters Thesis, Naval Postgraduate School, Monterey, CA, 1993.
5. Wirth, Walter M., *Linear Modeling of Rotorcraft Stability Analysis and Preliminary Design*, Masters Thesis, Naval Postgraduate School, Monterey, CA, 1993.
6. Hucke, William Jr., *Development of Graphical User Interface (GUI) and Capability Improvements for Joint Army/Navy Rotorcraft Analysis and Design (JANRAD) Software*, Masters Thesis, Naval Postgraduate School, Monterey, CA, 1998.
7. Hall, Stan, *Dynamic Modeling*, Sport Aviation, July 1987, pp. 30-36.
8. Popov, E. P., *Mechanics of Materials*, 2nd Ed., Prentice-Hall, Inc., Englewood Cliffs, NJ, 1976.
9. Vierck, Robert K., *Vibration Analysis*, 2nd Ed., Harper and Row Publishers, San Francisco, CA, 1979.
10. Wood, Edward R., *Class Notes, AA 3402 Helicopter Aerodynamics*, Naval Postgraduate School, Monterey, CA, 1996.
11. Abbott, Ira H. and Von Doenhoff, Albert E., *Theory of Wing Sections*, Dover Publishing, Inc., New York, 1959.
12. Anderson, John D., *Fundamentals of Aerodynamics*, 2nd Ed., McGraw-Hill, Inc., New York, 1991.
13. Greer, Daniel S., *Avionics System Development for Rotary Wing Unmanned Aerial Vehicle (UAV)*, Masters Thesis, Naval Postgraduate School, Monterey, CA, 1998.

INITIAL DISTRIBUTION LIST

1. Defense Technical Information Center.....2
8725 John J. Kingman Rd., STE 0944
Ft. Belvoir, VA 22060-6218
2. Dudley Knox Library.....2
Naval Postgraduate School
411 Dyer Rd.
Monterey, CA 93943-5101
3. Director, Training and Education1
MCCDC, Code C46
1019 Elliot Rd.
Quantico, VA 22134-5027
4. Director, Marine Corps Research Center2
MCCDC, Code C40RC
2040 Broadway Street
Quantico, VA 22134-5107
5. Director, Studies and Analysis Division1
MCCDC, Code C45
3300 Russell Road
Quantico, VA 22134-5130
6. Marine Corps Representative1
Naval Postgraduate School
Code 037, Bldg. 234, HA-220
699 Dyer Road
Monterey, CA 93940
7. Marine Corps Tactical Systems Support Activity1
Technical Advisory Branch
Attn: Maj. J. C. Cumiskey
Box 555171
Camp Pendleton, CA 92055-5080

8.	Dr. Russ W. Duren	2
	Department of Aeronautics and Astronautics, Code AA/DR	
	Naval Postgraduate School	
	Monterey, CA 93943-5101	
9.	Dr. E. Roberts Wood	1
	Department of Aeronautics and Astronautics, Code AA/Wd	
	Naval Postgraduate School	
	Monterey, CA 93943-5101	
10.	Chairman.....	2
	Department of Aeronautics and Astronautics, Code AA	
	Naval Postgraduate School	
	Monterey, CA 93943-5101	
11.	Matthew D. McEwen	2
	13 Mervine Street	
	Monterey, CA 93940	